PV Park Models in EMTP®

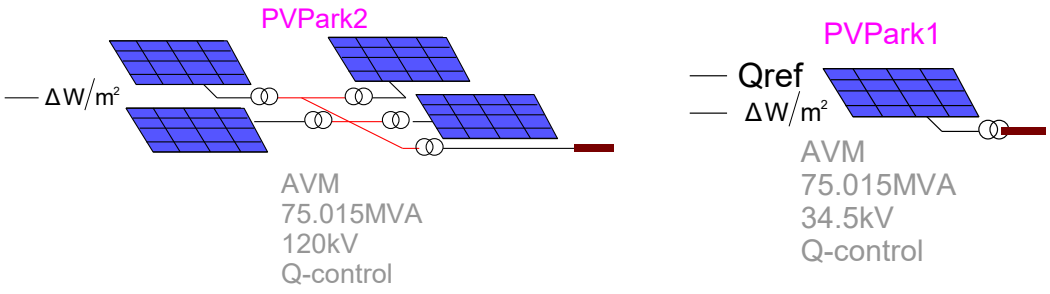

Prepared by:
Ulas Karaagac, Hossein Ashourian, Ilhan Kocar, Anton Stepanov, Henry Gras, Jean Mahseredjian

TABLE OF CONTENTS

Table of Figures

1 INTRODUCTION

This document presents generic EMTP models for Photovoltaic (PV) Park that can be used for stability analysis and interconnection studies.

Interconnecting a large-scale PV into the bulk power system has become a more important issue due to its significant impact on power system transient behavior. Failure to perform proper interconnection studies could lead to not only non-optimal designs and operations of PVs, but also severe power system operation and even stability problems. Manufacturer-specific models of PVs are typically favored for the interconnection studies due to their accuracy. However, these PV models have been typically delivered as black box model and their usage is limited to the terms of nondisclosure agreement. Utilities and project developers require accurate generic PV models to perform the preliminary grid integration studies before the actual design of the PV park is decided. Accurate generic PV park models will also enable the researchers to identify the potential PV grid integration issues and propose necessary countermeasures properly.

This PV park model is aggregated, the collector grid and the PV inverters are represented with their aggregated models. However, the model includes the park controller to preserve the overall control structure in the PV park. The inverters and the park control systems include the necessary nonlinearities, transient and protection functions to simulate the accurate transient behavior of the park to the external power system disturbances.

2 Model description

The EMT model presented in this document do not include the park transformer OLTC and any reactive power compensation device (such as Static VAR Compensator).

2.1 General

2.2 PV module

2.2.1 Parameters

This report presents the modeling of PV arrays in EMTP just by using the manufacturer's datasheet. The model is an equivalent electrical circuit with one nonlinear diode as illustrated in Figure 1:

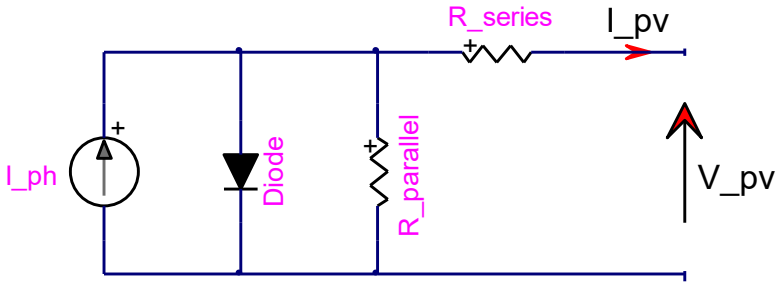

Figure 1 Equivalent circuit of a PV array

The electrical parameters of the components in the equivalent circuit are not readily available in datasheets. This report explains how to obtain the parameters using the datasheet information only and without performing any physical experiments.

First, the available information in datasheets, useful for the computation of parameters, is defined:

P_{max} : **Maximum power**

V_{maxP} : **Voltage at maximum power**

I_{maxP} : **Current at maximum power**

V_{oc} : **Open circuit voltage**

I_{sc} : **Short circuit current**

K_i : **Temperature coefficient of short circuit current**

K_v : **Temperature coefficient of open circuit voltage**

N_s : **Number of cells per module** (in series)

All these data are given for standard test conditions, obtained at a temperature of 25°C and for an irradiance of 1000 W/m².

$$T_{ref} = 25°C \qquad G_{ref} = 1000 W / m^2$$

One last data which is defined indirectly by the datasheet is the **ideal factor** a . This factor depends on the PV cell technology. A table in [1] gives the value of ideal factor for different PV technologies. This factor also varies with the irradiance [2], but the variation is low and it is considered constant in our model.

Finally, the actual atmospheric conditions are required: **temperature** T and **irradiance** G . Temperature is considered constant during time domain simulations given the time frame of typical EMT-type studies. The **irradiance**, however, can be constant or variable as defined by the user. More details are given at the end this document.

The relation between I_{PV} and V_{PV} in Figure 1 is given by:

$$I_{PV} = I_{ph} - I_{diode} - \frac{V_{PV} + I_{PV} R_s}{R_p} \quad (1)$$

where I_{diode} is the current flowing through the diode, R_s is the series resistance and R_p is the parallel resistance.

The next part explains how to obtain these electrical parameters.

2.2.2 Diode parameters

First, diode parameters need to be calculated using the standard conditions data (usually an irradiance of 1000 W/m2 and a temperature of 25°C).

$$I_{diode} = I_0 \left[\exp\left(\frac{V_{diode}}{a V_{th}} \right) - 1 \right] \quad (2)$$

where

$$V_{diode} = \frac{V_{PV} + I_{PV} R_s}{N_s} \quad (3)$$

The division by N_s is because we consider the diode for only one cell. As there are N_s cells in series, the voltage is equally divided on the N_s diodes.

The threshold voltage is:

$$V_{th} = \frac{k T_{ref}}{q} \quad (4)$$

where k is the Boltzmann's constant, q the charge of an electron and T_{ref} the reference temperature in Kelvin.

And the reversed saturation current is:

$$I_0 = \frac{I_{sc}}{\exp\left(\frac{V_{oc}}{a N_s V_{th}} \right) - 1} \quad (5)$$

From this, equation (1) becomes:

$$I_{PV} = I_{ph} - \frac{V_{PV} + I_{PV} R_s}{R_p} - I_0 \left[\exp\left(\frac{V_{PV} + I_{PV} R_s}{a N_s V_{th}} \right) - 1 \right] \quad (6)$$

In this equation there are still three unknown variables: I_{ph}, R_s and R_p.

To obtain these values the equations described in [3] are used. The equations are, however, solved here in a different way.

The goal here is to express I_{ph} and R_p in function of R_s. In such a case only one unknown variable remains, and the non-linear equation obtained can be solved with a numerical method.

Equation (6) is taken in maximum power conditions (voltage and current are given in datasheet) and from it a function f in function of R_s is defined:

$$f(R_s) = I_{ph} - I_{maxP} - \frac{V_{maxP} + I_{maxP} R_s}{R_p} - I_0 \left[\exp\left(\frac{V_{maxP} + I_{maxP} R_s}{a N_s V_{th}} \right) - 1 \right] \quad (7)$$

The objective here is to find such an R_s that the function f becomes zero.

2.2.3 Definition of R_p

To obtain this resistance another equation is required. The derivative of power with respect to voltage is used here. In maximal power condition, this derivative is zero.

$$0 = \left.\frac{dP_{PV}}{dV_{PV}}\right|_{max} = \left.\frac{d(V_{PV}I_{PV})}{dV_{PV}}\right|_{max} = I_{maxP} + V_{maxP}\left.\left(\frac{dI_{PV}}{dV_{PV}}\right)\right|_{max} \quad (8)$$

From (6) the derivative is calculated and taken in maximal power condition:

$$\left.\left(\frac{dI_{PV}}{dV_{PV}}\right)\right|_{max} = \frac{-aN_sV_{th} - R_pI_0\exp\left(\frac{V_{maxP}+I_{maxP}R_s}{aN_sV_{th}}\right)}{R_paN_sV_{th} + R_saN_sV_{th} + R_pR_sI_0\exp\left(\frac{V_{maxP}+I_{maxP}R_s}{aN_sV_{th}}\right)} \quad (9)$$

Equation (9) is inserted into (8) and R_p is isolated:

$$R_p = \frac{1}{\frac{I_{maxP}}{V_{maxP}-R_sI_{maxP}} - \frac{I_0}{aN_sV_{th}}\exp\left(\frac{V_{maxP}+I_{maxP}R_s}{aN_sV_{th}}\right)} \quad (10)$$

2.2.4 Definition of I_{ph}

As under short circuit conditions the voltage is low, the current flowing through the diode is negligible. In this case, there are only two resistances to be considered. As the short-circuit current is the one flowing in R_s we have:

$$I_{sc} = I_{ph}\frac{R_p}{R_s+R_p} \quad (11)$$

$$I_{ph} = I_{sc}\frac{R_s+R_p}{R_p} = I_{sc}\left(\frac{R_s}{R_p}+1\right) \quad (12)$$

By replacing R_p with (10):

$$I_{ph} = I_{sc}\left[1 + R_s\left(\frac{1}{\frac{V_{maxP}}{I_{maxP}}-R_s} - \frac{I_0}{aN_sV_{th}}\exp\left(\frac{V_{maxP}+I_{maxP}R_s}{aN_sV_{th}}\right)\right)\right] \quad (13)$$

After simplification:

$$I_{ph} = I_{sc}\left[\frac{V_{maxP}}{V_{maxP}-R_sI_{maxP}} - \frac{I_0R_s}{aN_sV_{th}}\exp\left(\frac{V_{maxP}+I_{maxP}R_s}{aN_sV_{th}}\right)\right] \quad (14)$$

2.2.5 Final Solution

The parallel resistance and the current source are now defined as a function of the series resistance. Equations (10) and (14) are inserted into (7):

$$\begin{aligned} f(R_s) = &-I_{maxP} + I_{sc}\left[\frac{V_{maxP}}{V_{maxP}-R_sI_{maxP}} - \frac{I_0R_s}{aN_sV_{th}}\exp\left(\frac{V_{maxP}+I_{maxP}R_s}{aN_sV_{th}}\right)\right] \\ &-(V_{maxP}+I_{maxP}R_s)\left[\frac{I_{maxP}}{V_{maxP}-R_sI_{maxP}} - \frac{I_0}{aN_sV_{th}}\exp\left(\frac{V_{maxP}+I_{maxP}R_s}{aN_sV_{th}}\right)\right] \\ &-I_0\left[\exp\left(\frac{V_{maxP}+I_{maxP}R_s}{aN_sV_{th}}\right)-1\right] \end{aligned} \quad (15)$$

This expression is simplified to:

$$f(R_s) = \frac{V_{maxP}(I_{sc} + I_0 - 2I_{maxP}) - I_0 I_{maxP} R_s}{V_{maxP} - R_s I_{maxP}} + I_0 \exp\left(\frac{V_{maxP} + I_{maxP} R_s}{aN_s V_{th}}\right)\left[\frac{R_s(I_{maxP} - I_{sc}) + V_{maxP} - aN_s V_{th}}{aN_s V_{th}}\right] \quad (16)$$

The goal is to find the value of R_s such that f equals to zero. To solve this non-linear equation, Newton method is used. As this function crosses zero several times, a specific interval has to be chosen. Newton method can be used because f' and f'' are both strictly positive on the studied interval: $[0; R_{s-\max}]$. $R_{s-\max}$ is defined as:

$$R_{s-max} = \frac{V_{oc} - V_{maxP}}{I_{maxP}} - \frac{aN_s V_{th}}{I_0} \exp\left(\frac{-V_{oc}}{aN_s V_{th}}\right) \quad (17)$$

Here is an example of the behaviour of $f(R_s)$ on $[0; R_{s-\max}]$ for a specific photovoltaic module (KC200GT Kyosera).

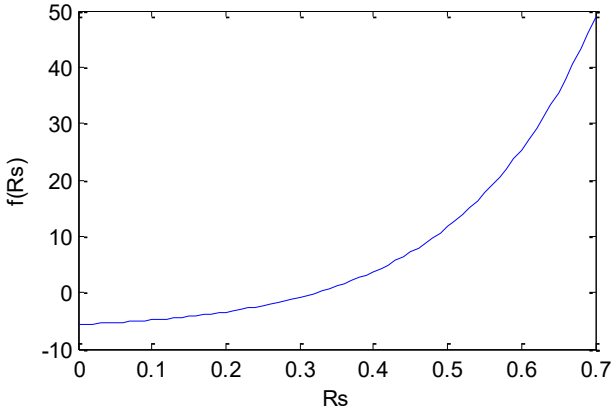

Figure 2 Behaviour of *f*(*Rs*) on studied interval

To use Newton method the derivative of the function is required:

$$\frac{df}{dR_s} = \frac{I_{maxP} V_{maxP}(I_{sc} - 2I_{maxP})}{(V_{maxP} - R_s I_{maxP})^2} + I_0 \exp\left(\frac{V_{maxP} + I_{maxP} R_s}{aN_s V_{th}}\right)\left[\frac{-I_{sc} aN_s V_{th} + R_s I_{maxP}(I_{maxP} - I_{sc}) + I_{maxP} V_{maxP}}{(aN_s V_{th})^2}\right] \quad (18)$$

As f' is positive, initialization is done with the maximum value:

$$R_s^0 = R_{s-max} \quad (19)$$

The iterative procedure is:

$$R_s^{i+1} = R_s^i - \frac{f(R_s^i)}{f'(R_s^i)} \quad (20)$$

And it is stopped when the variation is below the tolerance ε :

$$R_s^i - R_s^{i+1} < \varepsilon \quad (21)$$

Once the iterative procedure yields the final value of R_s^i, it is possible to compute R_p and I_{ph} using equations (10) and (14).

As previous calculations were done under standard conditions, the current of the current source is abbreviated with I_{ph0}.

Parameters are now calculated for the actual atmospheric conditions:

$$V_{th} = \frac{kT}{q} \tag{22}$$

$$I_0 = \frac{I_{sc} + K_i(T - T_{ref})}{\exp\left(\frac{V_{oc} + K_v(T - T_{ref})}{aN_s V_{th}}\right) - 1} \tag{23}$$

$$I_{ph\_T} = I_{ph0} + K_i\left(T - T_{ref}\right) \tag{24}$$

$$I_{ph} = I_{ph\_T}\frac{G}{G_{ref}} \tag{25}$$

Here we have the parameters for the given conditions but for only one photovoltaic module. The total number of modules is calculated using the nominal DC voltage and the given output power of the plant.

$$N_{mod-s} = \frac{V_{DC}}{V_{maxP}} \qquad N_{mod-p} = \frac{P_{plant}}{V_{DC} I_{maxP}} \tag{26}$$

where N_{mod-p} is the number of module in parallel and N_{mod-s} the number of module in series in the plant.

Parameters are updated for the last time:

$$I_{ph\_tot} = I_{ph}\, N_{mod-p} \tag{27}$$

$$R_{s\_tot} = \frac{N_{mod-s}}{N_{mod-p}} R_s \qquad R_{p\_tot} = \frac{N_{mod-s}}{N_{mod-p}} R_p \tag{28}$$

$$I_{0\_tot} = N_{mod-p} I_0 \qquad N_{s\_tot} = N_s\, N_{mod-s} \tag{29}$$

$$I_{diodes} = I_{0\_tot} \exp\left(\frac{V_{diodes}}{aN_{s\_tot} V_{th}}\right) \tag{30}$$

Subscript “tot” is used to indicate that it is the final value that will be used in the model.
All electrical parameters are sent into the circuit.

3 Electrical circuit

The EMTP circuit is presented in Figure 3.
As the diode is a non-linear device, it is moved inside the control block, so the current source showed in Figure 3 represents the photoelectric current source in parallel with the diode.

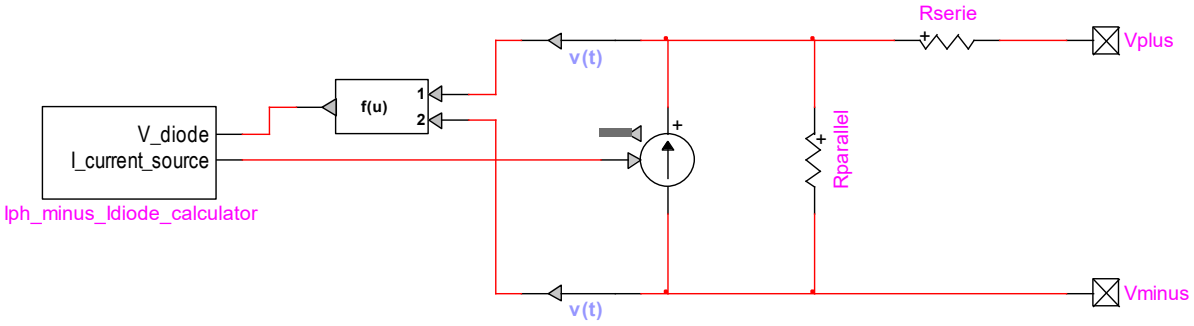

Figure 3 Equivalent electrical circuit of PV park

The control block calculates the current from photoelectric cells and the current flowing through the diode. Then the diode current is subtracted from photoelectric current, and the resulting current drives the controlled current source in Figure 3.

Figure 4 presents the subcircuit which calculates the photovoltaic current as a function of irradiance with respect to (25) and the diode current as a function of the diode voltage using (30). The irradiance can be varied from outside of the PV park device. The temperature is considered constant during the simulation.

An option to force the DC link voltage to a nominal value is available. In this case, the PV cell device is an ideal voltage source.

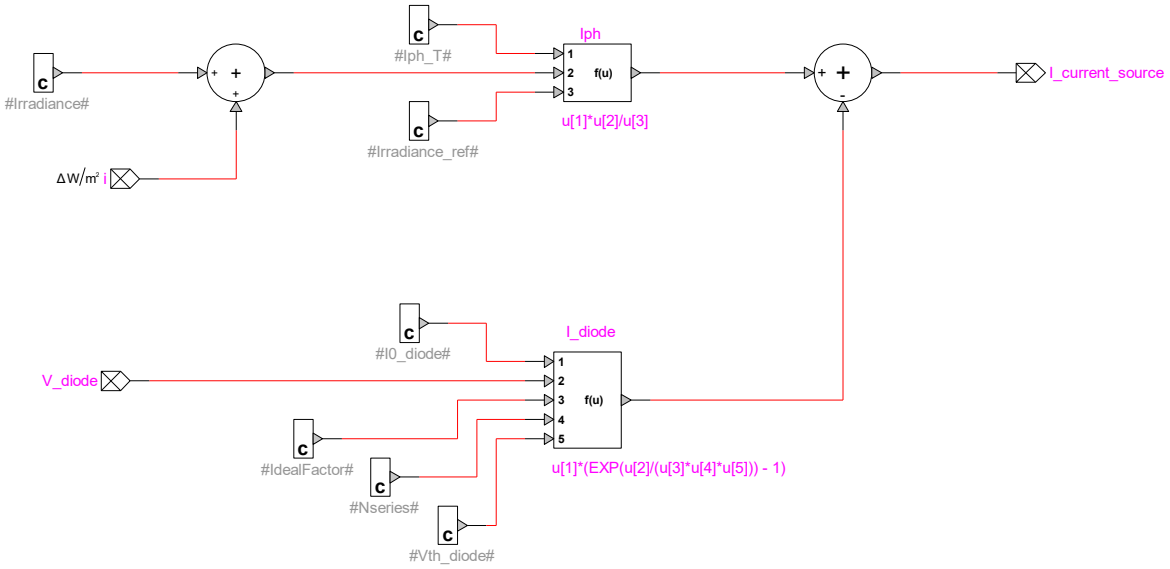

Figure 4 Current source subcircuit

3.1 Reactive Power Control in PV Parks

The active power at the point of interconnection depends on the weather conditions. However, according to customary grid code requirements, the PV park should have a central PV park controller (PVPC) to control the reactive power at POI.

The PV park reactive power control is based on the secondary voltage control concept [9]. At primary level, the inverter controller monitors and controls its own positive sequence terminal voltage (V_{wt}^{+}) with a proportional voltage regulator. At secondary level, the PVPC monitors the reactive power

at POI (Q_{POI}) and control it by modifying the PV inverters reference voltage values (V') via a proportional-integral (PI) reactive power regulator as shown in Figure 5. In Figure 5 and hereafter, all variables are in pu (unless opposite is stated) and the apostrophe sign is used to indicate the reference values coming from the controllers.

A Q(V) mode is available where the Q-reference is function of the voltage.

Although not shown in Figure 5, the PVPC may also contain voltage control (V-control) and power factor control (PF-control) functions. When PVPC is working under V-control function, the reactive power reference in Figure 5 (Q'_{POI}) is calculated by an outer proportional voltage control, i.e.

$$Q_{POI} = K_{Vpoi}\left(V'_{POI} - V^{+}_{POI}\right) \tag{31}$$

where V^{+}_{POI} is the positive sequence voltage at POI and K_{Vpoi} is the PVPC voltage regulator gain.

When PVPC is working under PF-control function, Q'_{POI} is calculated using the active power at POI (P_{POI}) and the desired power factor at POI (pf_{POI}).

When a severe voltage sag occurs at POI (due to a fault), the PI regulator output ($\Delta U'$) is kept constant by blocking the input ($Q'_{POI} - Q_{POI}$) to avoid overvoltage following the fault removal.

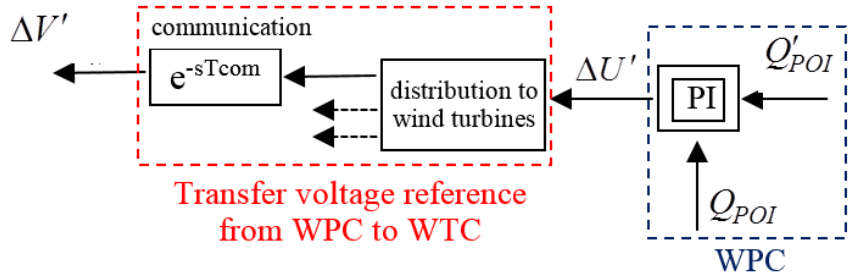

Figure 5 Reactive power control at POI (Q-control function)

3.2 PV inverter control and protection systems

The considered topology is shown in Figure 6. It uses a dc-ac converter system consisting of a voltage source converter (VSC) on the grid side (GSC: Grid Side Converter). The dc resistive chopper is used for the dc bus overvoltage protection. A line inductor (choke filter) and an ac harmonic filter are used at the GSC to improve the power quality.

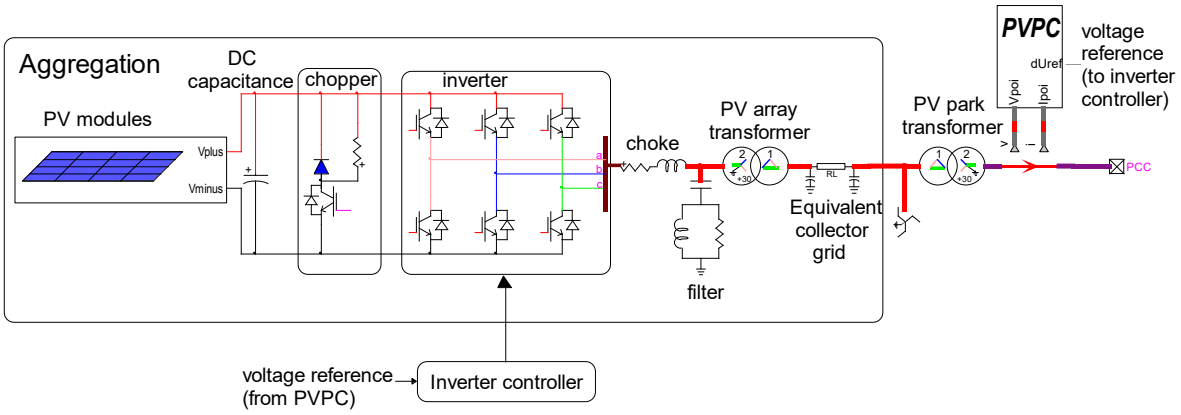

Figure 6 PV park configuration

The simplified diagram of PV inverter control and protection system is shown in Figure 7. The sampled signals are converted to per unit and filtered at “Measurements & Filters” block. The input measuring filters are low-pass (LP) type.

- “Compute Variables” block computes the variables used by the PV inverter control and protection system.
- “Protection System” block contains low voltage and overvoltage relays, GSC overcurrent protections and dc resistive chopper control.

The control of the PV inverter is achieved by controlling the GSC utilizing vector control techniques. Vector control allows decoupled control of real and reactive powers. The currents are projected on a rotating reference frame based on either ac flux or voltage. Those projections are referred to d- and q-components of their respective currents. In flux-based rotating frame, the q-component corresponds to real power and the d-component to reactive power. In voltage-based rotating frame (90^0 ahead of flux-based frame), the d and q components represent the opposite.

The control scheme is illustrated in Figure 8. In this figure, i_{qg} and i_{dg} are the q- and d-axis currents of the GSC, V_{dc} is the dc bus voltage, and V_{wt}^{+} is the positive sequence voltage at PV park transformer MV terminal.

In the control scheme presented in Figure 8, the GSC operates in the stator voltage reference (SVR) frame. i_{dg} is used to maintain V_{dc} and i_{qg} is used to control V_{wt}^{+}.

The GSC is controlled by a two-level controller. The slow outer control calculates the reference dq-frame currents (i'_{dg} and i'_{qg}) and the fast inner control allows controlling the converter ac voltage reference that will be used to generate the modulated switching pattern.

The reference for the positive sequence voltage at FSC transformer MV terminal (V') is calculated by the PVPC (see Figure 5).

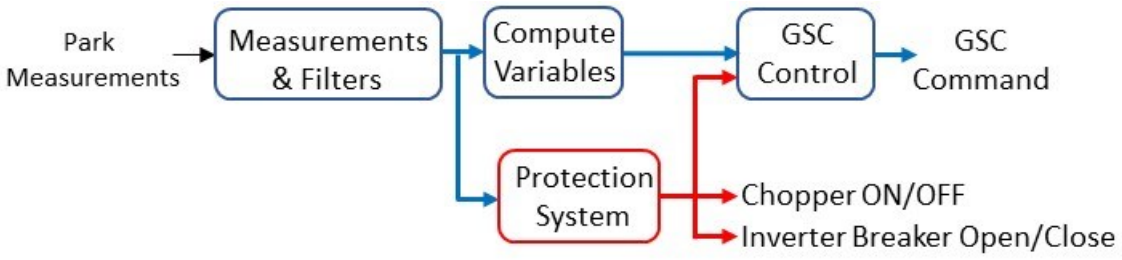

Figure 7 Simplified diagram of inverter control and protection system

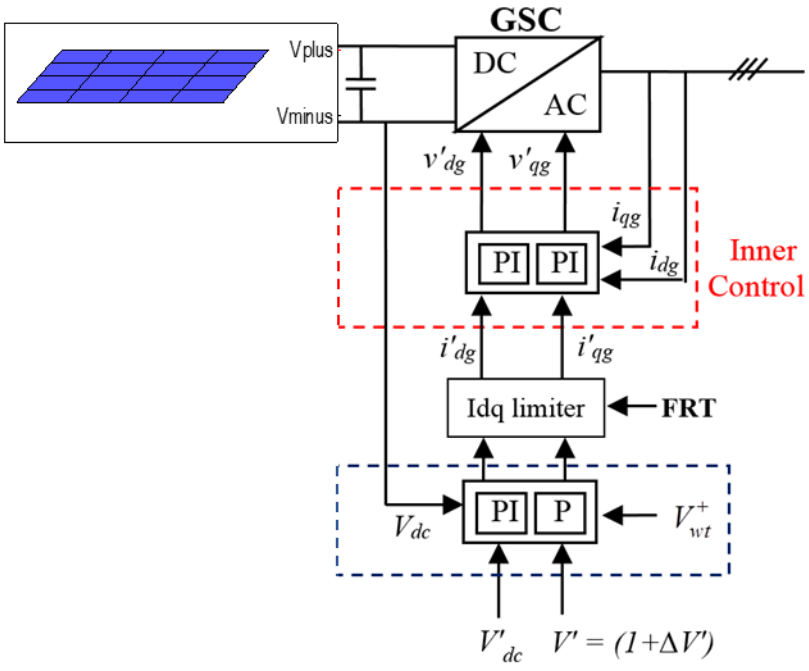

Figure 8 Schematic diagram of inverter control

4 EMTP IMPLEMENTATION

The developed PV park model setup in EMTP is encapsulated using a subcircuit with a programmed mask as illustrated in Figure 9 and Figure 10. The model consists of a solar panel, a LV/MV PV array transformer, equivalent PI circuit of the collector grid and a MV/HV PV park transformer (see Figure 6).

The first tab of the PV park mask allows the user to modify the general PV park parameters (**number of PV arrays** in the PV park, POI and collector **grid voltage levels**, **collector grid equivalent** and **zig-zag transformer** parameters (if it exists)), the general PV array parameters (**PV array rated power**, **voltage** and **frequency**), the PV park operating conditions (**number of PV arrays in service**, **PVPC operating mode** and **reactive power** at POI) and the atmospheric conditions.

In the Atmospheric conditions section, the maximum capacity of the park is calculated. If Power-control is selected, the PV park operates at a reference power. The power is limited by the maximum PV park capacity. If MPPT-control is selected, the PV park operates at maximum capacity for the conditions specified in the Atmospheric conditions section. Warning: The MPPT controller is not modelled in the version so if the irradiance is varied during the simulation, the power reference does not change.

The second and the third tab is used for MV/HV PV park transformer and LV/MV PV array transformer parameters, respectively.

The forth tab is used to modify the parameters of converter control system given below:

- **Sampling rate and PWM frequency at PV converters**
- **PV inverter input measuring filter parameters**,
- **GSC control parameters**,
- **Coupled / Decoupled sequence control option for GSC**

The fifth tab is used to modify the parameters of voltage sag, chopper and overcurrent protections. The sixth tab is used to modify the PVPC parameters.

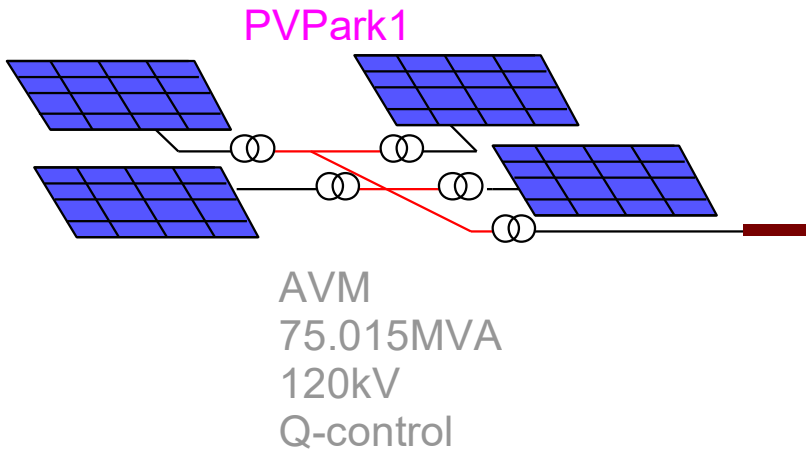

Figure 9 PV park device, mask parameters shown in Figure 10

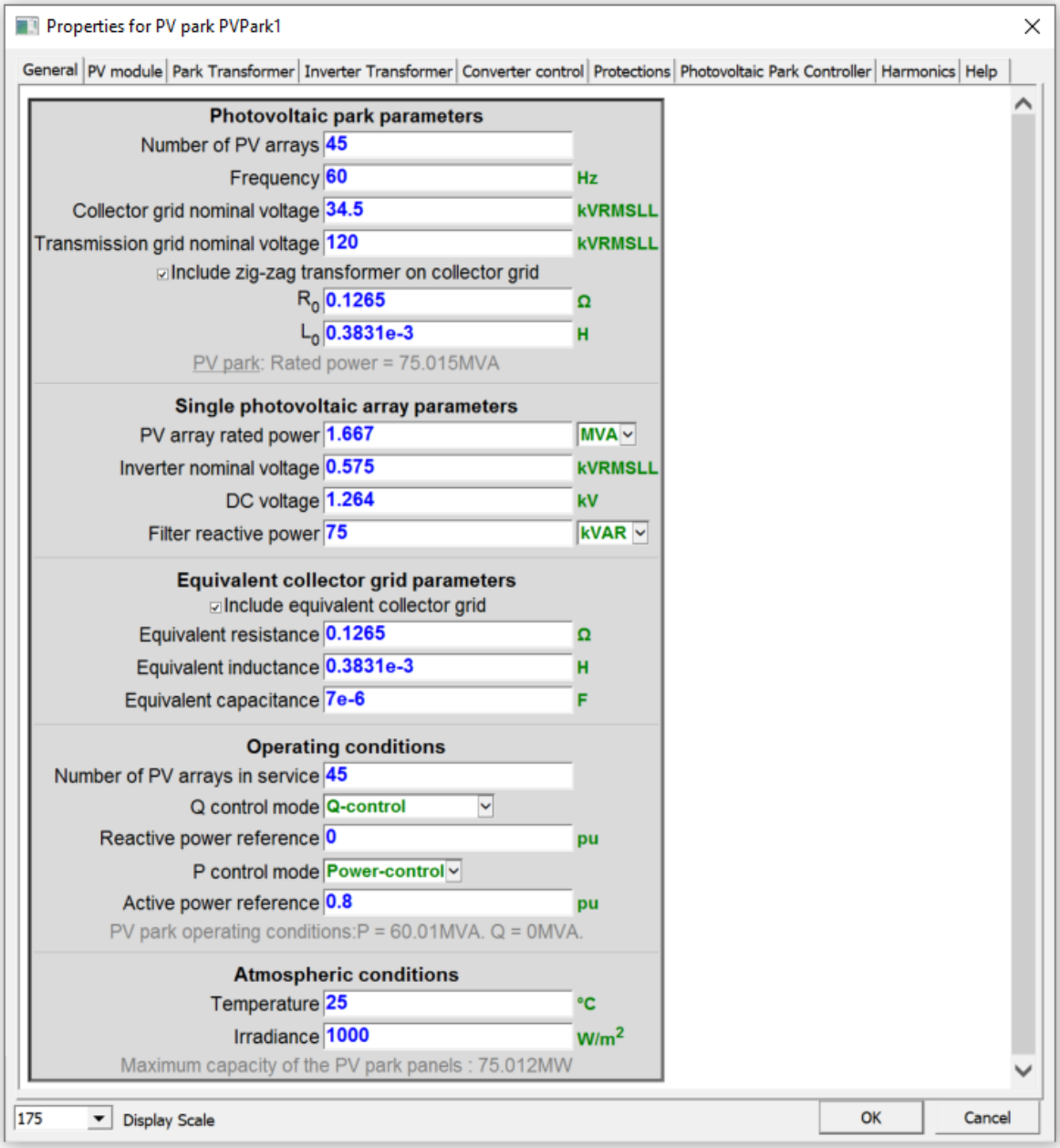

Figure 10 PV park device mask

4.1 Detailed (DM) and Average Value (AVM) Converter Models

The EMTP diagram of the PV dc-ac converter system detailed model (DM) is shown in Figure 11. A detailed two-level topology (Figure 12.a) is used for the VSCs in which the valve is composed by one IGBT switch, two non-ideal (series and anti-parallel) diodes and a snubber circuit as shown in Figure 12.b. The non-ideal diodes are modeled as non-linear resistances. The DC resistive chopper limits the DC bus voltage and is controlled by protection system block.

The PWM block in ac-dc-ac converter system EMTP diagram receives the three-phase reference voltages from converter control and generates the pulse pattern for the six IGBT switches by comparing the voltage reference with a triangular carrier wave. In a two-level converter, if the reference voltage is higher than the carrier wave then the phase terminal is connected to the positive DC terminal, and if it

is lower, the phase terminal is connected to the negative DC terminal. The EMTP diagram of the PWM block is presented in Figure 13.

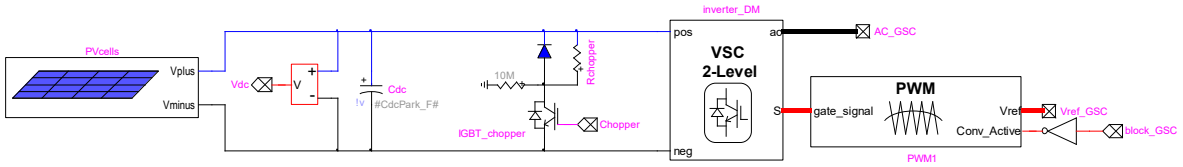

Figure 11 EMTP® diagram of dc-ac converter system block in PV models (detailed model version)

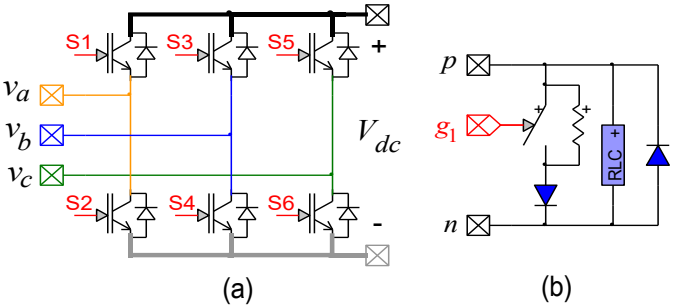

Figure 12 (a) Two-level Converter, (b) IGBT valve

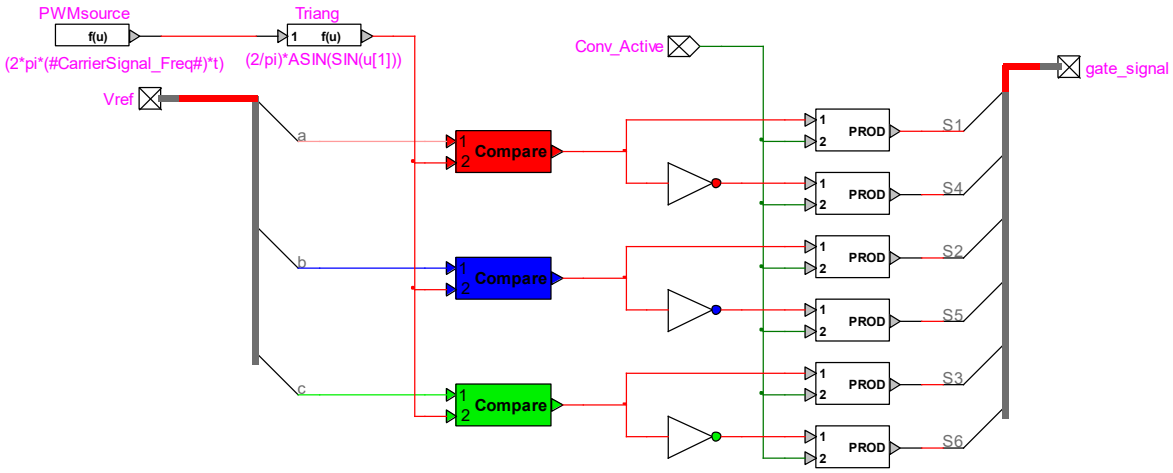

Figure 13 PWM control block

The DM mimics the converter behavior accurately. However, simulation of such switching circuits with variable topology requires many time-consuming mathematical operations and the high frequency PWM signals force small simulation time step usage. These computational inefficiencies can be eliminated by using average value model (AVM) which replicates the average response of switching devices, converters and controls through simplified functions and controlled sources [11]. AVMs have been successfully developed for wind and solar generation technologies [12], [13]. AVM obtained by replacing DM of converters with voltage-controlled sources on the ac side and current-controlled sources on the dc side as shown in Figure 14 and Figure 15.

The forth (converter control) tab of the PV park device mask (see Figure 10) enables used AVM-DM selection.

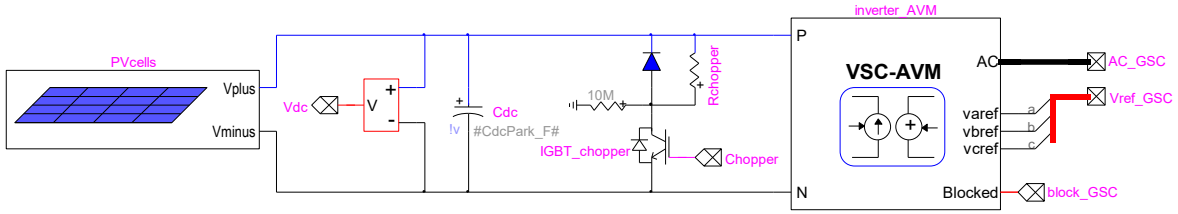

Figure 14 dc-ac converter system block in PV models (average value model version)

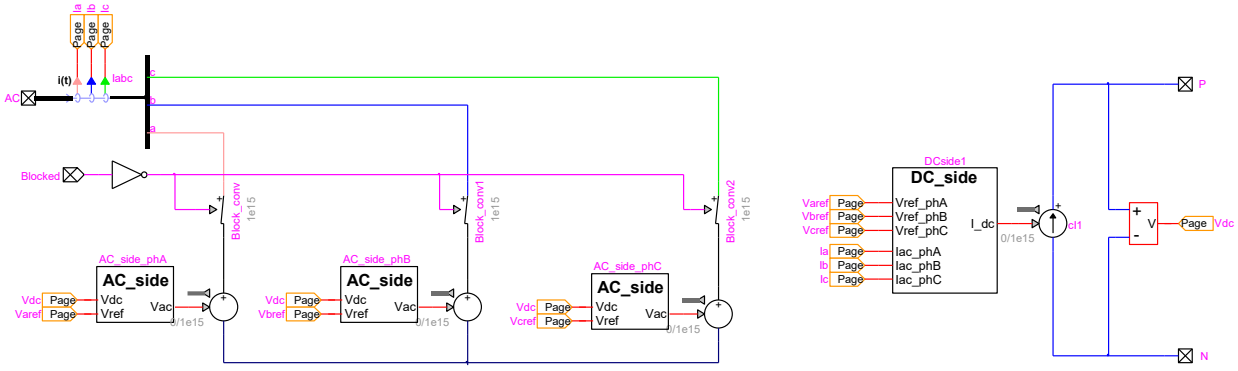

Figure 15 EMTP® diagram of AVM Representation of the VSC

4.2 PV park Model in EMTP

The EMTP diagram of the PV park is shown in Figure 16. It is composed of

- “PV hardware” block which contains the PV panel and the inverter,
- “PV Control System” block,
- “PV park Controller” block,
- PI circuit that represents equivalent collector grid,
- PV converter transformer (converter_transformer),
- PV park transformer,
- Initialization Sources with load flow (LF) constraint.
- A Norton harmonic source for harmonic analysis.

The initialization source contains the load flow constraint. Depending if the park operating mode, the bus is changed from PV (for V-mode) to PQ (for the other modes). It also prevents large transients at external network during initialization of PV electrical and control systems.

A capacitor bank device is present in the circuit but excluded. Users can include is and modify the parameters. If the name is not modified, the capacitor will be considered for power flow initialization.

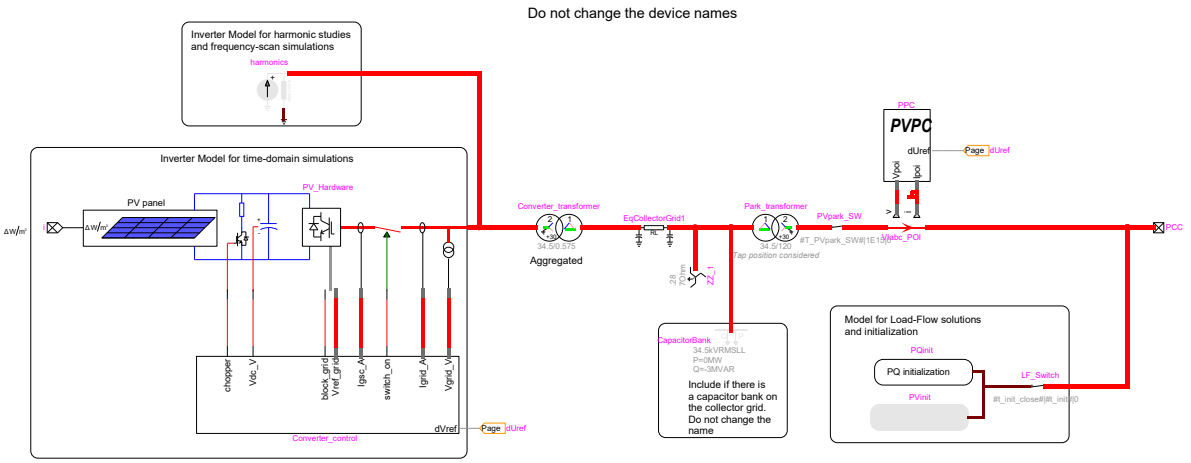

Figure 16 EMTP® diagram of the PV park

4.2.1 PV park Control System Block

The function of PVPC is to adjust the PV inverter controller voltage reference in order to achieve desired reactive power at POI (see Figure 5). The “PVPC” block consists in measuring block, an outer voltage (or power factor) control and a slow inner proportional-integral reactive power control as shown in Figure 17. The measuring block receives the voltages and the currents at POI (i.e. HV terminal of PV farm transformer) and calculates voltage magnitude, active power and reactive power. The reactive power reference for the inner proportional-integral reactive power control is produced either by the outer proportional voltage control (V-control) or by the outer power factor control (pf-control) unless Q-control is selected.

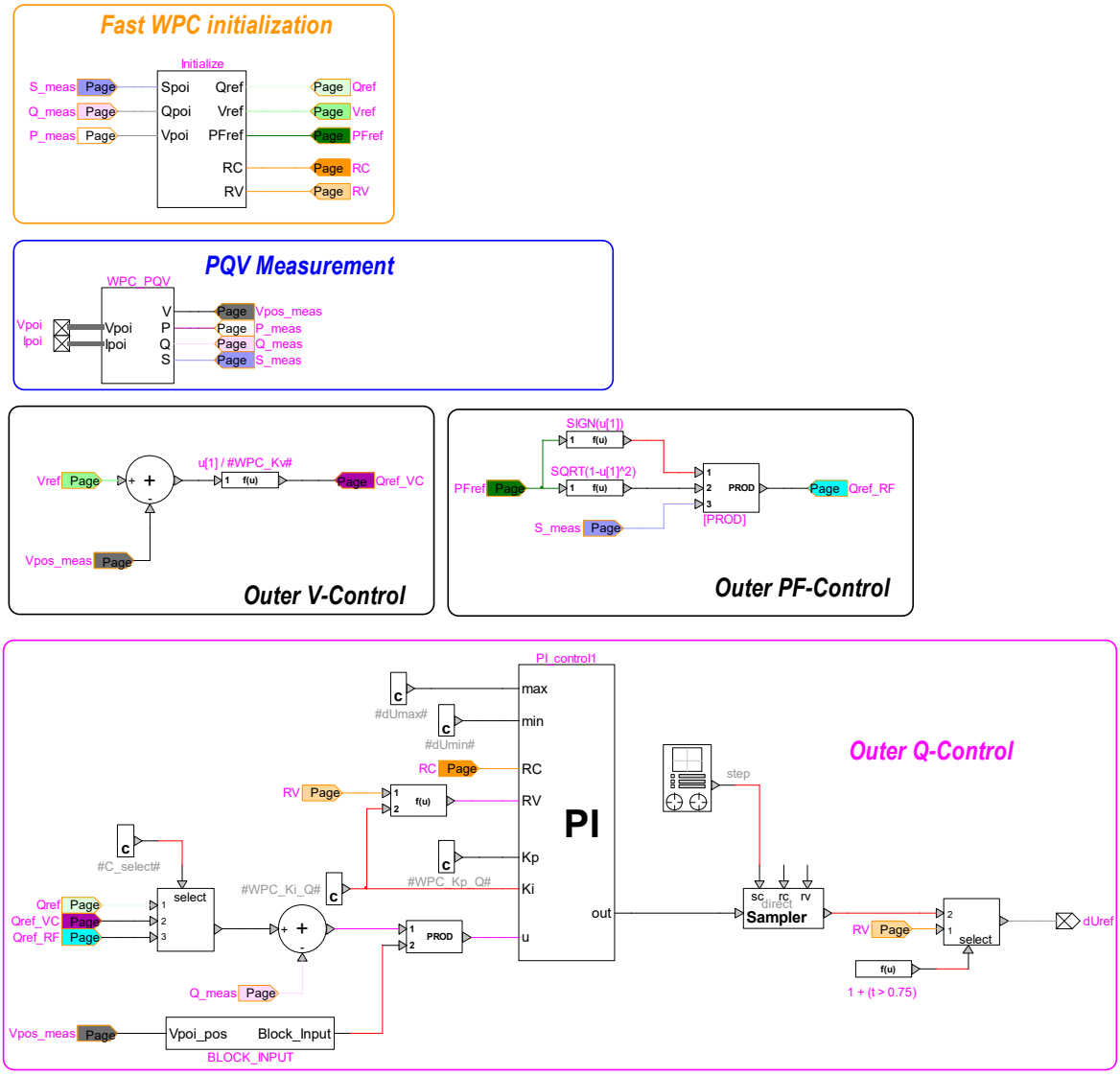

Figure 17 EMTP® diagram of "PVPC" (PV park controller) block

4.2.2 PV Electrical System

The EMTP diagram of the electrical system is composed of the PV panel, the dc-ac converter system, the choke filter, the shunt ac harmonic filters, the PV array transformer and the PV park transformer as shown in Figure 18.

The measurement blocks are used for monitoring and control purposes. The monitored variables are GSC and total PV unit currents, and FC terminal voltages. The dc voltage is also monitored (in dc-ac converter system block). All variables are monitored as instantaneous values and meter locations and directions are shown in Figure 18.

The dc-ac converter system block details have been presented in Section 4.1.

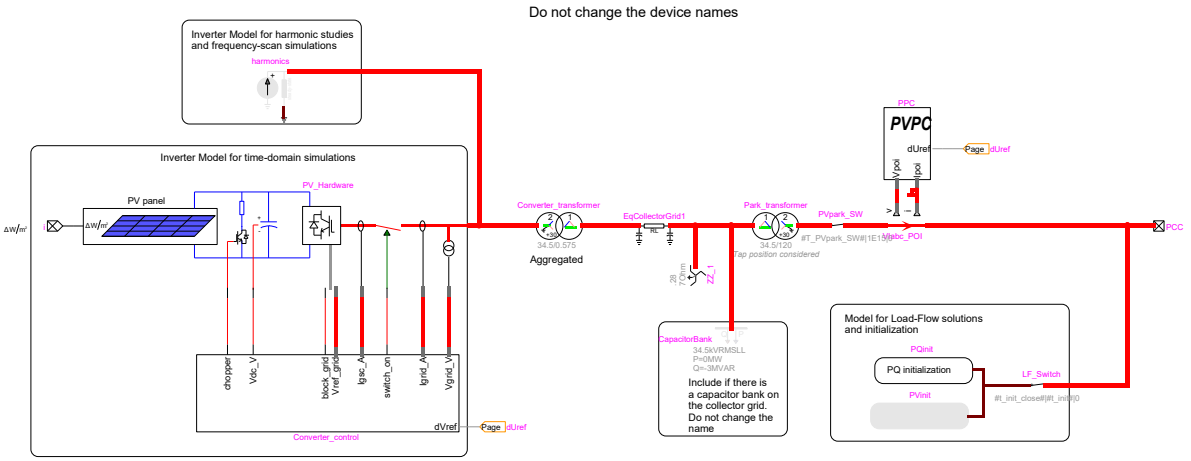

Figure 18 EMTP® diagram of the PV park

The “shunt ac harmonic filters” block includes two band-pass filters as shown in Figure 19. These filters are tuned at switching frequencies harmonics n_1 and n_2. The filter parameters are computed as

$$C_{f1} = \frac{Q_{filter}\ N_{wt}}{U^2(2\pi f)} \tag{32}$$

$$L_{f1} = \frac{N_{wt}}{C_{f1}(2\pi f\, n_1)^2} \tag{33}$$

$$R_{f1} = \frac{(2\pi f)n_1\ L_{f1}\ Q}{N_{wt}} \tag{34}$$

$$C_{f2} = C_{f1} \tag{35}$$

$$L_{f2} = \frac{N_{wt}}{C_{f2}(2\pi f\, n_2)^2} \tag{36}$$

$$R_{f2} = \frac{(2\pi f)n_2\ L_{f2}\ Q}{N_{wt}} \tag{37}$$

where U is the rated LV grid voltage, Q_{filter} is the **reactive power of the filter** and Q is the **quality factor**.

The switching frequencies harmonics n_1 and n_2 are as follows

$$n_1 = f_{PWM-gsc} \,/\, f_s \tag{38}$$

$$n_2 = 2n_1 \tag{39}$$

where $f_{PWM-gsc}$ is the **PWM frequency** at GSC and f_s is the **nominal frequency**.

In case another type of filter or other parameters should be used, the filter can be modified by the user inside the PV park subcircuit. If several PV parks are found in the network, the filter subcircuit and its parents must be made unique to avoid modifying all PV park instances.

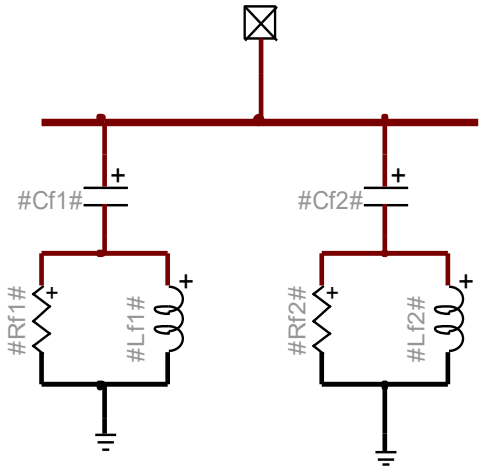

Figure 19 "shunt ac harmonic filter" block

4.2.3 PV inverter Control System Block

The EMTP diagram of the PV inverter control system block is shown in Figure 20. The sampled signals are converted to pu and filtered. The sampling frequency are set to 12.5 kHz from device mask as shown in Figure 10 and can be modified by the user. The "sampling" blocks are deactivated in AVM due to large simulation time step usage. In generic model, 2nd order Bessel type low pass filters are used. The cut-off frequencies of the filters are set to 2.5 kHz and can be modified by the user. The order (up to 8th order), the type (Bessel and Butterworth) and the cut-off frequencies of the low pass filters can be modified from device mask as shown in Figure 10. The "GSC Compute Variables" block does the dq transformation required for the vector control. The GSC ("Grid Control" block) operates in the stator voltage reference frame. The protection block includes the over/under voltage relay, the deep voltage sag detector, the dc chopper control and overcurrent detector.

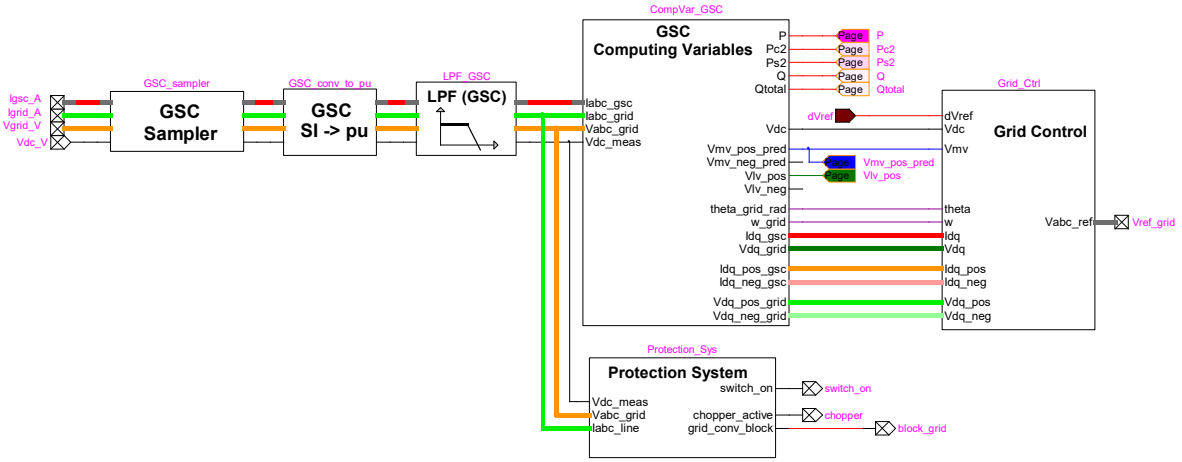

Figure 20 EMTP® diagram of the PV inverter control block

The transformation matrix T in (40) transforms the phase variables into two quadrature axis (d and q reference frame) components rotating at synchronous speed $\omega = d\theta / dt$. The phase angle θ of the rotating reference frame is derived by the double synchronous reference frame (DSRF) PLL [14] (see Figure 21) from the PV inverter terminal voltages allowing the synchronization of the control parameters with the system voltage. In matrix T, the direct axis d is aligned with the stator voltage.

$$T = \frac{2}{3}\begin{bmatrix} \cos(\omega t) & \cos(\omega t - 2\pi/3) & \cos(\omega t + 2\pi/3t) \\ -\sin(\omega t) & -\sin(\omega t - 2\pi/3) & -\sin(\omega t + 2\pi/3) \\ 1/2 & 1/2 & 1/2 \end{bmatrix} \quad (40)$$

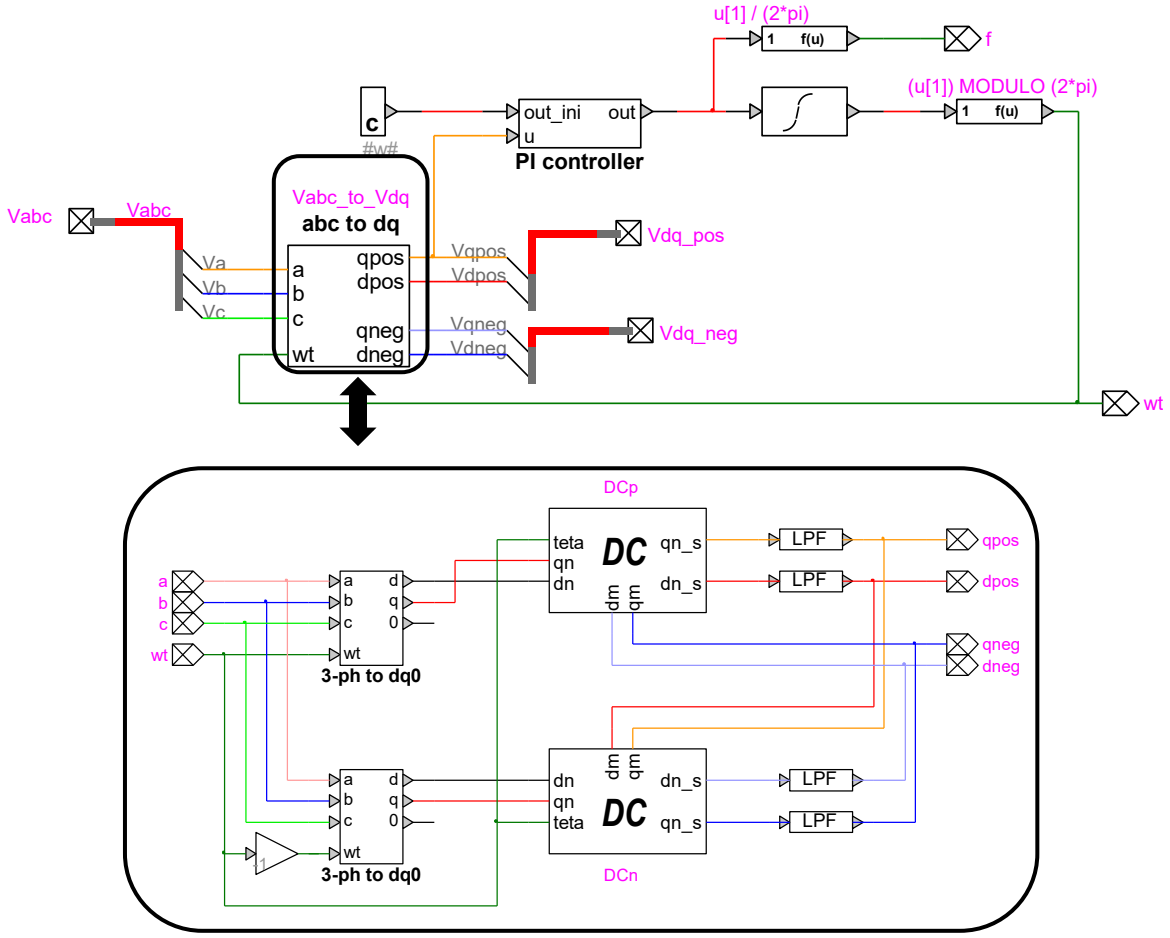

Figure 21 EMTP® diagram of DSRF PLL

4.2.3.1 PV inverter Grid Side Converter Control

The function of GSC is maintaining the dc bus voltage V_{dc} at its nominal value and controlling the positive sequence voltage at MV side of PV array transformer (V_{wt}^{+}).The EMTP diagram of the "Grid Control" block is shown in Figure 22. GSC control offers both coupled and decoupled sequence control options. User can select the GSC control option from the device mask as shown in Figure 12.

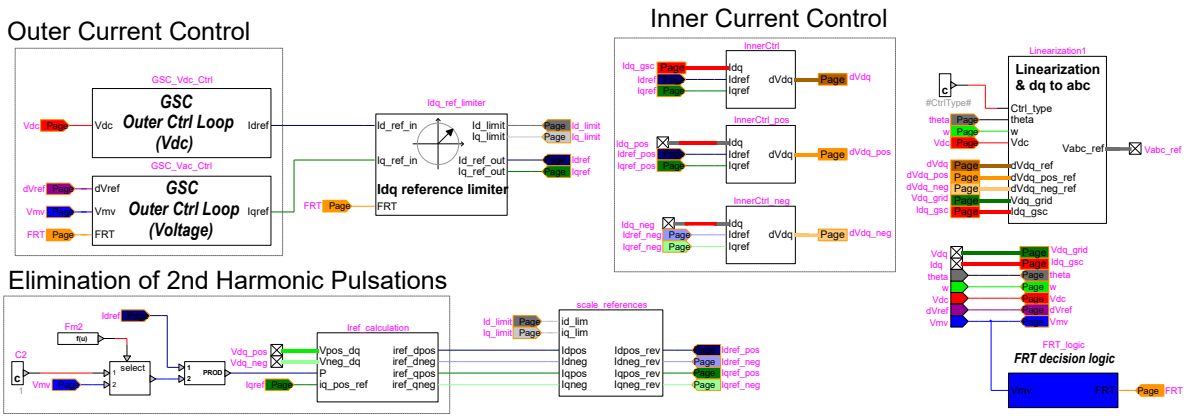

Figure 22 EMTP® diagram of PV inverter "Grid Control" block

4.2.3.1.1 PV inverter GSC Coupled Control

The q-axis reference current is calculated by the proportional outer voltage control.

$$i'_{qg} = K_V \left(V' - V^+_{wt} \right) \tag{41}$$

where K_V is the voltage regulator gain. The reference for MV side of PV array transformer positive sequence voltage (V') is calculated by the PVPC (see Figure 5).

The positive sequence voltage at MV side of PV array transformer is not directly measured by the PV inverter controller and it is approximated by

$$V^+_{wt} = \left(V^+_{dwt} \right)^2 + \left(V^+_{qwt} \right)^2 \tag{42}$$

where

$$V^+_{dwt} = \tilde{V}^+_{dwt} + R_{tr}\tilde{I}^+_{dwt} - X_{tr}\tilde{I}^+_{qwt} \tag{43}$$

$$V^+_{qwt} = \tilde{V}^+_{qwt} + R_{tr}\tilde{I}^+_{qwt} + X_{tr}\tilde{I}^+_{dwt} \tag{44}$$

In (42) - (44), V^+_{dwt} and V^+_{qwt} are the d-axis and q-axis positive sequence voltage at MV side of PV array transformer, $\tilde{V}^+_{dwt}$ and $\tilde{V}^+_{qwt}$ are the d-axis and q-axis positive sequence voltage at PV inverter terminals (i.e. the d-axis and q-axis positive sequence voltage at LV side of PV array transformer), $\tilde{I}^+_{dwt}$ and I^+_{qwt} are the d-axis and q-axis positive sequence currents of PV inverter (i.e. the d-axis and q-axis positive sequence currents at LV side of PV array transformer), R_{tr} and X_{tr} are the resistance and reactance values of the PV array transformer.

The d-axis reference current is calculated by the proportional outer dc voltage control. It is a PI controller tuned based on inertia emulation.

$$k_p = \omega_0^2 \left(2H_{Cdc} \right) \tag{45}$$

$$k_i = 2\xi\omega_0 \left(2H_{Cdc} \right) \tag{46}$$

where ω_0 is the natural frequency of the closed loop system and ξ is the damping factor. $H_{Cdc} = \left(E_{Cdc} / S_{wt}\right)$ is the static moment of inertia, E_{Cdc} is the stored energy in dc bus capacitor (in Joules) and S_{wt} is the PV park rated power (in VA).

The schematic of the GSC connected to the power system is shown in Figure 23. $Z = R + j\omega L$ represents the grid impedance including the transformers as well as the choke filter of the GSC. The voltage equation is given by

$$\mathbf{v_{abc}} = \mathbf{R}\ \mathbf{i_{gabc}} - \mathbf{L}\left(d\ \mathbf{i_{gabc}} / dt\right) + \mathbf{v_{gabc}} \tag{47}$$

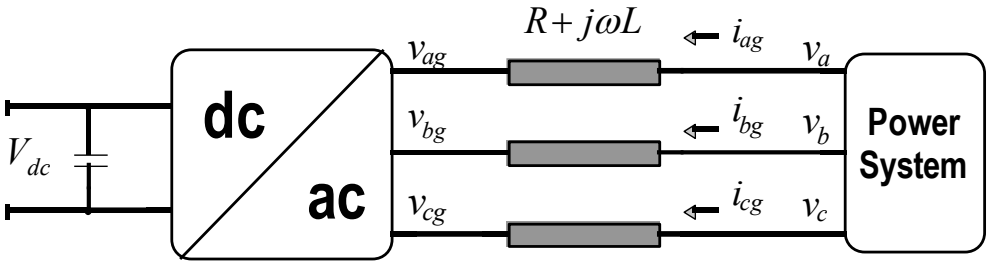

Figure 23 GSC arrangement

The link between GSC output current and voltage can be described by the transfer function

$$G_{gsc}(s) = 1/\left(R + sL\right) \tag{48}$$

Using [15], the PI controller parameters of the inner current control loop are found as

$$k_p = \alpha_c L \tag{49}$$

$$k_i = \alpha_c R \tag{50}$$

.

The feed-forward compensating terms $\omega L_{choke} i_{qg} + v_{d-choke}$ and $\left(-\omega L_{choke} i_{dg} + v_{q-choke}\right)$ are added to the d- and q-axis voltages calculated by the PI regulators, respectively. The converter reference voltages are as follows

$$v'_{dg} = -\left(k_p + k_i / s\right)\left(i'_{dg} - i_{dg}\right) + \omega L_{choke} i_{qg} + v_{d-choke} \tag{51}$$

$$v'_{qg} = -\left(k_p + k_i / s\right)\left(i'_{qg} - i_{qg}\right) - \omega L_{choke} i_{dg} + v_{q-choke} \tag{52}$$

During normal operation, the controller gives the priority to the active currents, i.e.

$$\begin{aligned} i'_{dg} &< I_{dg}^{\lim} \\ i'_{qg} &< I_{qg}^{\lim} = \sqrt{\left(I_g^{\lim}\right)^2 - \left(i'_{dg}\right)^2} \end{aligned} \tag{53}$$

where $I_{dg}^{\lim}$, $I_{qg}^{\lim}$ and $I_g^{\lim}$ are the limits for d-axis, q-axis and total GSC currents, respectively.

The PV inverters are equipped with an FRT function to fulfill the grid code requirement regarding voltage support shown in Figure 24. The FRT function is activated when

$$\left|1-V_{wt}^{+}\right| > V_{FRT-ON} \tag{54}$$

and deactivated when

$$\left|1-V_{wt}^{+}\right| < V_{FRT-OFF} \tag{55}$$

after a pre-specified release time t_{FRT} .

When FRT function is active, the GSC controller gives the priority to the reactive current by reversing the d- and q-axis current limits given in (53), i.e.

$$\begin{aligned} i'_{qg} &< I_{qg}^{\lim} \\ i'_{dg} &< I_{dg}^{\lim} = \sqrt{\left(I_{g}^{\lim}\right)^2 - \left(i'_{qg}\right)^2} \end{aligned} \tag{56}$$

The EMTP diagram of “Idq reference limiter” and “FRT decision logic” blocks are given in Figure 25 and Figure 26, respectively. The limits for d-axis, q-axis and total GSC currents and FRT function thresholds can be modified from the device mask as shown in Figure 12.

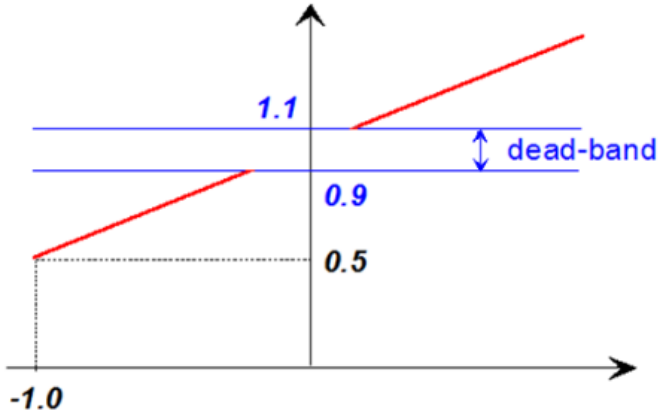

Figure 24 PV inverter reactive output current during voltage disturbances [16].

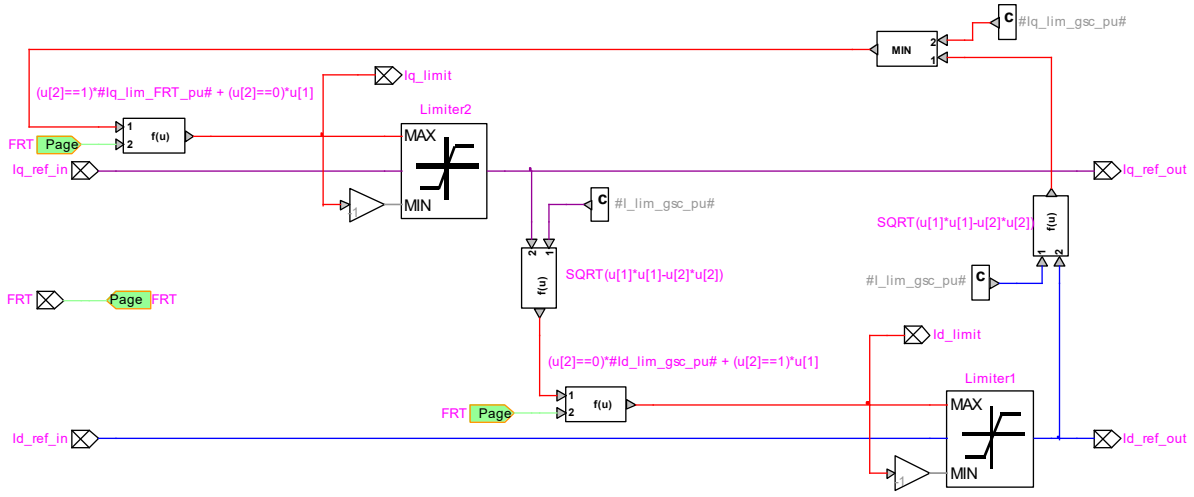

Figure 25 EMTP® diagram of “Idq reference limiter” block

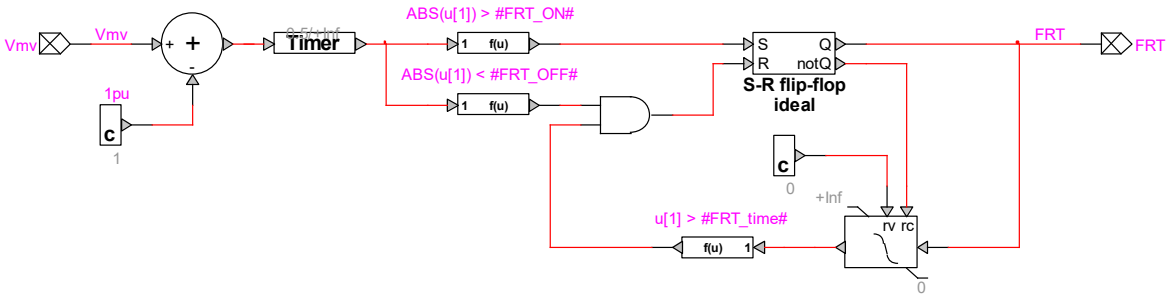

Figure 26 EMTP® diagram of "FRT decision logic" block

4.2.3.1.2 PV inverter Grid Side Converter Decoupled Sequence Control

Ideally, the GSC control presented in the previous section is not expected to inject any negative sequence currents to the grid during unbalanced loading conditions or faults. However, the terminal voltage of PV inverter contains negative sequence components during unbalanced loading conditions or faults. This causes second harmonic power oscillations in GSC power output. The instantaneous active and reactive powers such unbalanced grid conditions can be also written as [17]

$$\begin{aligned} p &= P_0 + P_{C2}\cos(2\omega t) + P_{S2}\cos(2\omega t) \\ q &= Q_0 + Q_{C2}\cos(2\omega t) + Q_{S2}\cos(2\omega t) \end{aligned} \tag{57}$$

where P_0 and Q_0 are the average values of the instantaneous active and reactive powers respectively, whereas P_{C2}, P_{S2}, Q_{C2} and Q_{S2} represent the magnitude of the second harmonic oscillating terms in these instantaneous powers.

With decoupled sequence control usage, four of the six power magnitudes in (57) can be controlled for a given grid voltage conditions. As the oscillating terms in active power P_{C2}, P_{S2} cause oscillations in dc bus voltage V_{dc}, the GSC current references ($i_{dg}^{+\prime}$, $i_{qg}^{+\prime}$, $i_{dg}^{-\prime}$, $i_{qg}^{-\prime}$) are calculated to cancel out these terms (i.e. $P_{C2} = P_{S2} = 0$).

The outer control and Idq limiter shown in Figure 8 calculates i'_{dg}, i'_{qg}, $I_{dg}^{\lim}$ and $I_{qg}^{\lim}$. These values are used to calculate the GSC current references $i_{dg}^{+\prime}$, $i_{qg}^{+\prime}$, $i_{dg}^{-\prime}$ and $i_{qg}^{-\prime}$ for the decoupled sequence current controller. As the positive sequence reactive current injection during faults is defined by the grid code (see Figure 24), the GSC current reference calculation in [17] is modified as below:

$$\begin{bmatrix} i_{qg}^{+\prime} \\ i_{dg}^{+\prime} \\ i_{qg}^{-\prime} \\ i_{dg}^{-\prime} \end{bmatrix} = \begin{bmatrix} 1 & 0 & 0 & 0 \\ v_{qg}^{+} & v_{dg}^{+} & v_{qg}^{-} & v_{dg}^{-} \\ v_{qg}^{-} & v_{dg}^{-} & v_{qg}^{+} & v_{dg}^{+} \\ -v_{dg}^{-} & v_{qg}^{-} & v_{dg}^{+} & -v_{qg}^{+} \end{bmatrix}^{-1} \begin{bmatrix} i'_{qg} \\ P_0 \\ P_{C2} \\ P_{S2} \end{bmatrix} \tag{58}$$

where P_0 is approximated by

$$P_0 = V_{wt}^{+}\ i'_{dg} \tag{59}$$

The calculated reference values in (58) is revised considering the converter limits $I_{dg}^{\lim}$ and $I_{qg}^{\lim}$. For example when $\left(i_{qg}^{+}{}' + i_{qg}^{-}{}'\right) > I_{qg}^{\lim}$, the q-axis reference current references are revised as below

$$\begin{aligned} i_{qg}^{+}{}'' &= i_{qg}^{+}{}' \left[I_{qg}^{\lim} \Big/ \left(i_{qg}^{+}{}' + i_{qg}^{-}{}'\right)\right] \\ i_{qg}^{-}{}'' &= i_{qg}^{-}{}' \left[I_{qg}^{\lim} \Big/ \left(i_{qg}^{+}{}' + i_{qg}^{-}{}'\right)\right] \end{aligned} \tag{60}$$

where I_{qg}^{+}'' and I_{qg}^{-}'' are the revised reference values for q-axis positive and negative currents, respectively.

The revised d-axis positive and negative current references I_{dg}^{+}'' and I_{dg}^{-}'' can be obtained with the same approach using $I_{dg}^{\lim}$. It should be emphasized here that, during faults the priority is providing I_{dg}^{+} specified by the grid code. The remaining reserve in GSC is used for eliminating P_{C2} and P_{S2}. Hence, its performance reduces with the decrease in electrical distance between the PV park and the unbalanced fault location.

As i_{dg}^{+}, i_{qg}^{+}, i_{dg}^{-} and i_{qg}^{-} are controlled, the decoupled sequence control contains four PI regulator and requires sequence extraction for GSC currents and voltages. The sequence decoupling method [18] shown in Figure 27 is used in EMTP implementation. In this method, a combination of a low-pass filter (LPF) and double line frequency Park transform (P^{-2} and P^{+2}) is used to produce the oscillating signal, which is then subtracted. The blocks C and P represent the Clarke and Park transformation matrices, and the superscripts ±1 and ±2 correspond to direct and inverse transformation at line frequency and double line frequency, respectively.

In EMTP implementation, the feed-forward compensating terms $\left(\omega L_{choke} i_{qg} + v_{d-choke}\right)$ and $\left(-\omega L_{choke} i_{dg} + v_{q-choke}\right)$ are kept in coupled form and added to the PI regulator outputs in stationary αβ-frame.

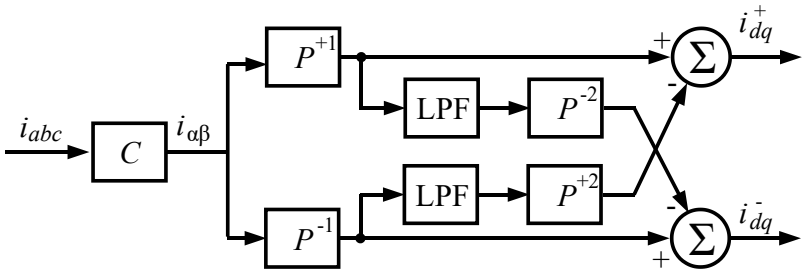

Figure 27 Sequence extraction using decoupling method.

4.2.4 PV inverter Protection System Block

Figure **28** shows the “protection system” block. It includes overvoltage and undervoltage protection relays, a dc overvoltage protection (chopper protection) and an overcurrent detector for each converter

to protect IGBT devices when the system is subjected to overcurrent. For initialization, all protection systems, except for DC chopper protection, are activated after 100ms of simulation (i.e. init_Prot_delay = 0.1s). The protection system parameters can be modified from the device mask as shown in Figure 29.

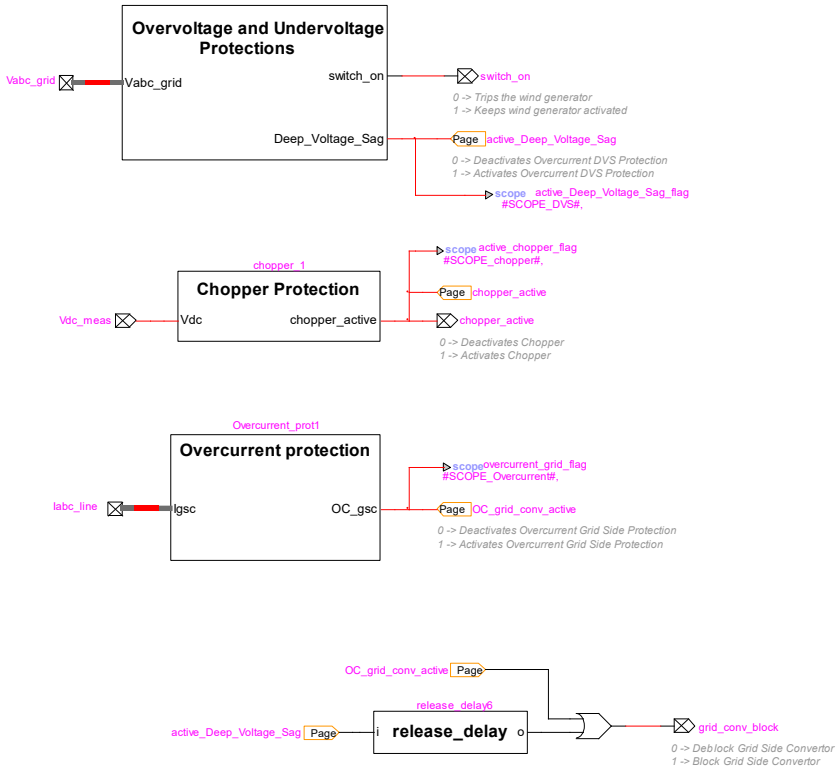

Figure 28 **EMTP® diagram of protection system block**

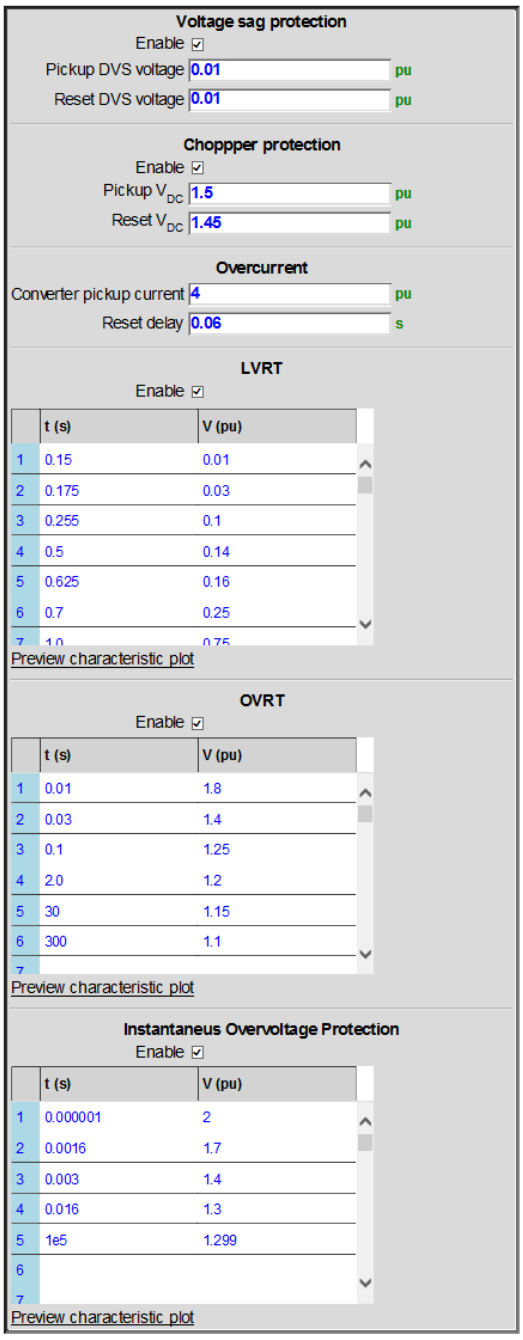

Figure 29 Protection system parameters

4.2.4.1 Overvoltage and Undervoltage protections

Figure **30** shows overvoltage and undervoltage protections. It includes rms-based over/under voltage relays, cumulative instantaneous overvoltage relays, deep voltage sag detectors.

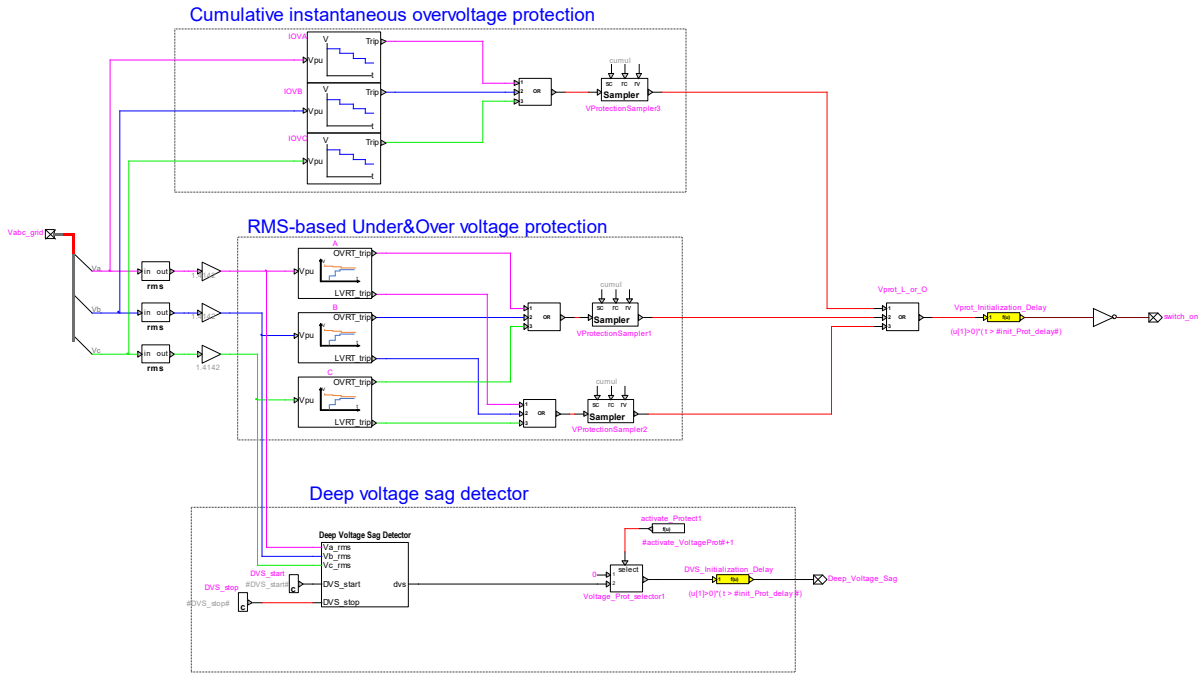

Figure 30 **EMTP® diagram of overvoltage and undervoltage protections**

The instantaneous overvoltage protection suggested by IEEE Std 1547-2018 is developed and added to the protection schemes. This protection works based on a cumulative instantaneous overvoltage. Figure 31 shows the threshold values of the voltage (per unit of nominal instantaneous peak base) and cumulative duration of the transient overvoltage protection, and they can be modified in the device mask. The cumulative duration is the sum of durations when the instantaneous voltage exceeds the protection threshold over a one-minute time window.

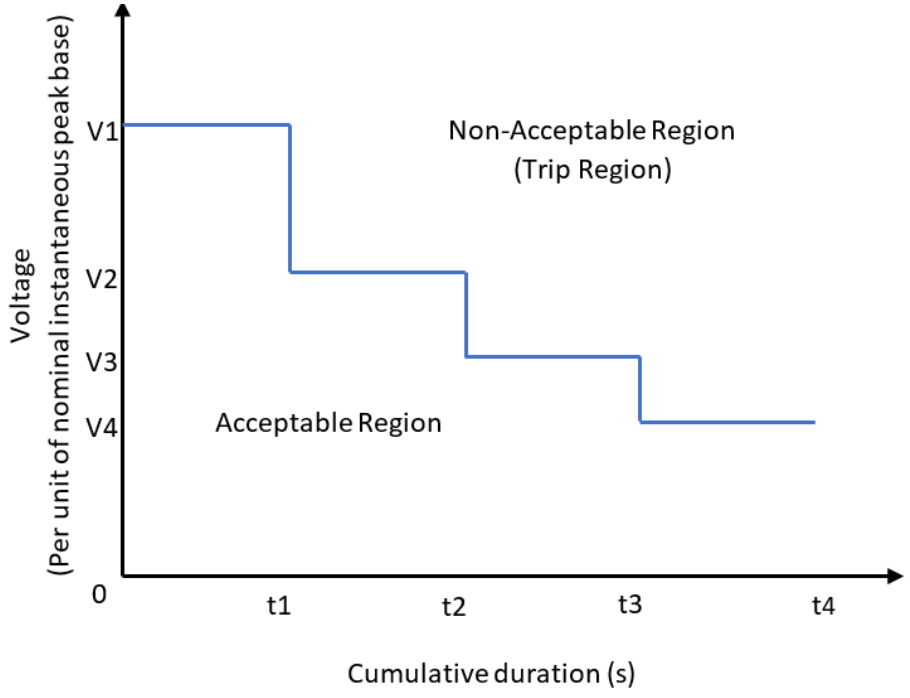

Figure 31 Transient overvoltage limits

The RMS-based over/under voltage protections are designed based on the technical requirements set by Hydro Quebec for the integration of renewable generation. The over/under voltage limits as a function of time are presented in Figure 32 and can be modified in the PV device mask. The voltages below the red line reference and above the black line reference correspond to the ride-through region where the PV park is supposed to remain connected to the grid. This block measures the rms voltages on each phase and sends a trip signal to the PV inverter circuit breaker when any of the phase rms voltage violates the limits in Figure 32.

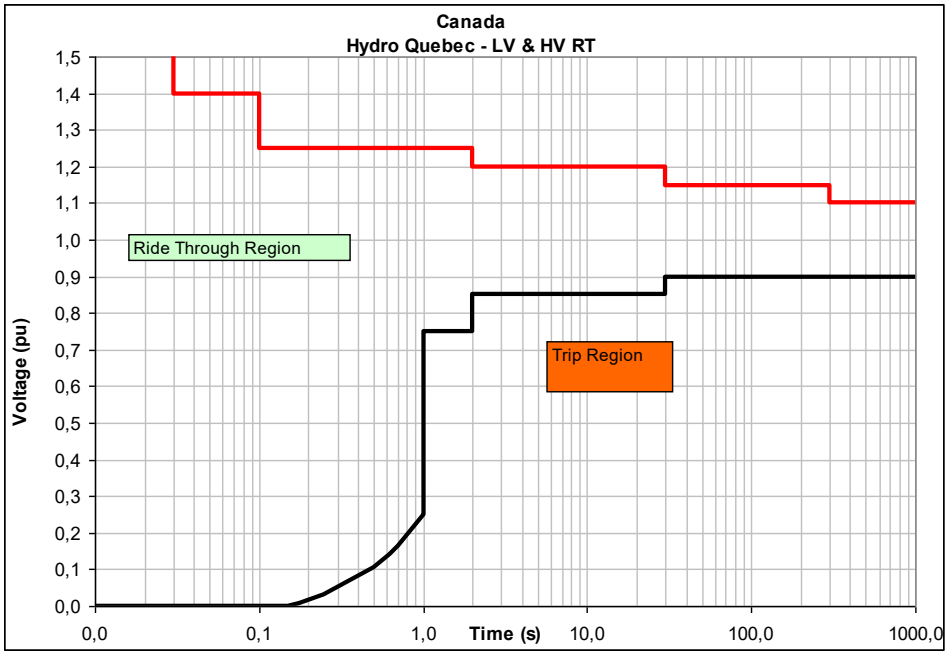

Figure 32 LVRT and HVRT requirements [19]

The “Deep Voltage Sag Detector” block temporary blocks the GSC in order to prevent potential overcurrents and restrict the FRT operation to the faults that occur outside the PV park.

4.2.4.2 dc Overvoltage Protection Block

The function of dc chopper is to limit the dc bus voltage. It is activated when the dc bus voltage exceeds $\left|U_{chopper-ON}\right|$ and deactivated when dc bus reduces below $\left|U_{chopper-OFF}\right|$. EMTP diagram of the “dc overvoltage protection” is shown in Figure 33.

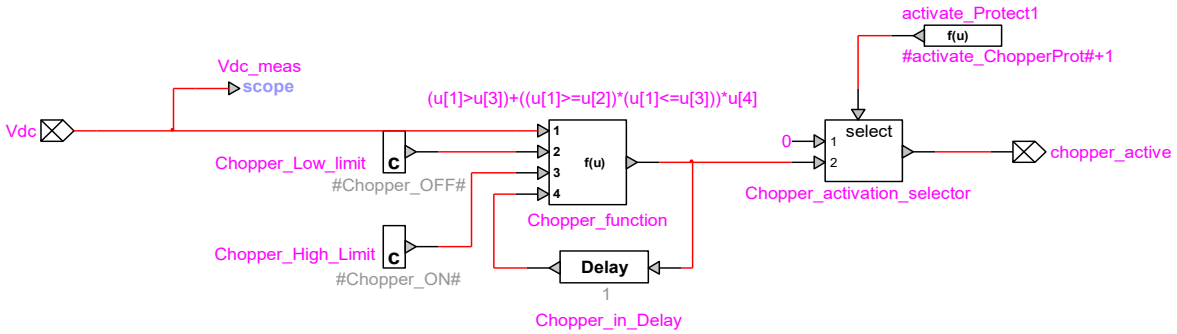

Figure 33 EMTP® diagram of dc overvoltage protection block

4.2.4.3 Overcurrent Protection Block

The overcurrent protection shown in Figure 34 blocks the converter temporarily when the converter current exceeds the pre-specified limit.

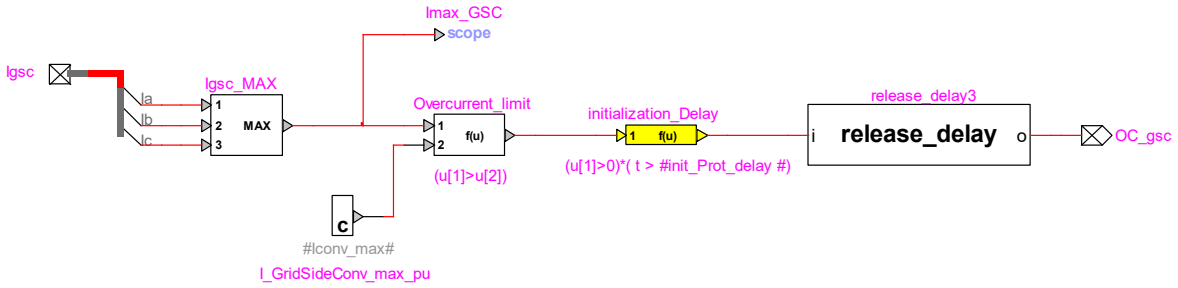

Figure 34 EMTP® diagram of overcurrent protection block

4.2.5 PV harmonic model

For harmonic analysis, the PV park is modeled with a harmonic Norton source. The harmonic study can be done in time domain, in which case **Use harmonic model for steady-state and time-domain simulations** must be checked or in the frequency domain with the frequency-scan simulation option, in which case **Use harmonic model for frequency-scan simulations**.

The harmonic currents are provided in percentage of the fundamental, for one inverter. The total park current is rescaled according to the number of inverters in service.

It is possible to automatically adjust the fundamental frequency current generated by each inverter and the harmonic current angles to match the load-flow results by checking **Adjust fundamental frequency current to match Load-Flow results**. When this box is checked, the **I Angle** input of the first line, which corresponds to the fundamental frequency current is adjusted to match the inverter current angle during the load-flow. The **Fundamental frequency current magnitude** is also adjusted to match the load-flow results. The fundamental frequency angle value is also added to the **I Angle** values of the other harmonics. Therefore, when this option is checked, the phase difference between the harmonic currents and the fundamental frequency current should be entered in the **I Angle** column.

5 PV PARK RESPONSE TO UNBALANCED FAULTS

This section provides a comparison between the PV park responses with coupled and decoupled sequence controls. Although the comparison is conducted for various type unbalanced faults in the 120 kV, 60 Hz test system shown in Figure 35 [28]-[30], only the 250 ms double line to ground (DLG) fault simulation scenarios are presented. The simulation scenarios are presented in Table I. The PV converters are represented with their AVMs. The simulation time step is 10 μs.

In the test system, the loads are represented by equivalent impedances connected from bus to ground on each phase. The transmission lines are represented by constant parameter models and transformers with saturation. The equivalent parameters for the 34.5 kV equivalent feeders are calculated on the basis of active and reactive power losses in the feeder for the rated current flow from each of the PVs [31]. In all simulations, the PV is operating at full load with unity power factor (i.e. Q_{POI} = 0).

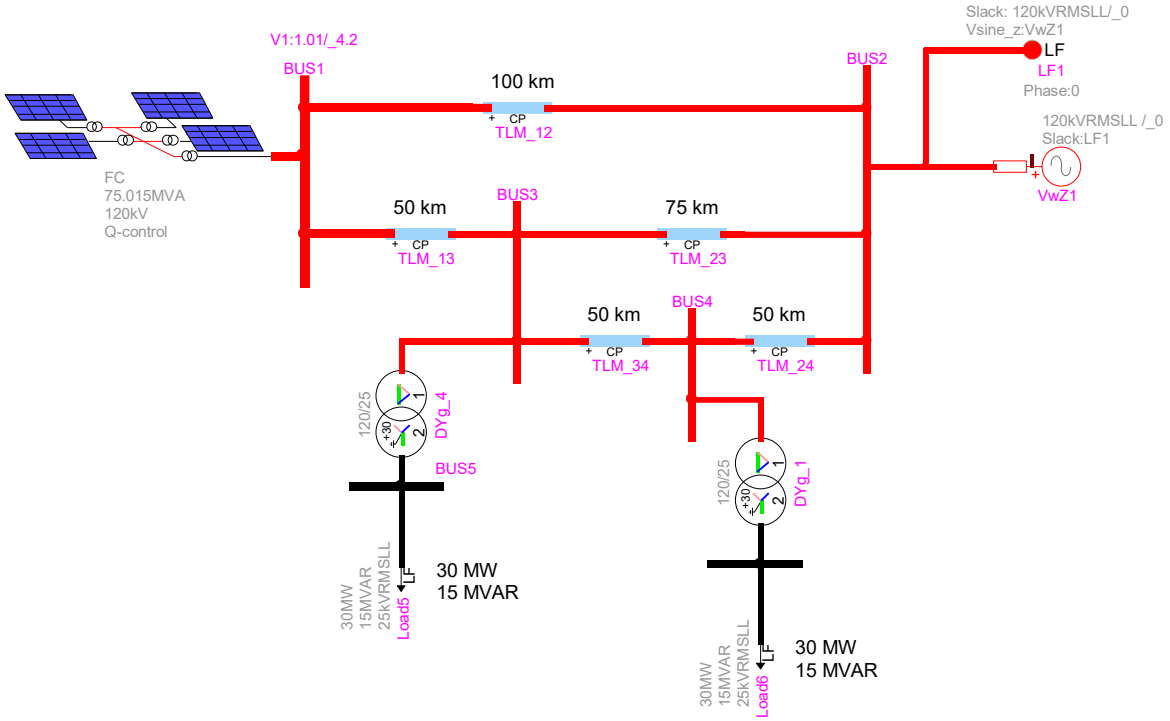

Figure 35 120 kV, 60 Hz test system

Table I Simulation Scenarios

Scenario	Fault Location	GSC Control Scheme
M1	BUS4	Coupled Control
M2	BUS4	Decoupled Sequence Control
N1	BUS6	Coupled Control
N2	BUS6	Decoupled Sequence Control

5.1 PV park Response to Unbalanced Faults

5.1.1 Simulation Scenarios M1 and M2 with PV park

As shown in Figure 36, the simulated unbalanced fault results in second harmonic pulsations in the active power output of the PV park in scenario M1. These second harmonic pulsations are eliminated in scenario M2 with decoupled sequence control scheme in GSC at the expense of a reduction in the active power output of PV park as shown in Figure **37**. On the other hand, the reactive power output of the PV park is similar in scenarios M1 and M2. This is due to the strict FRT requirement on positive sequence reactive currents.

The performance of GSC decoupled sequence control is limited to GSC rating as well as the FRT requirement specified by the grid code. The complete elimination of second harmonic pulsations cannot be achieved when the required GSC current output exceeds its rating. It should be noted that, when the electrical distance between the PV park and unbalanced fault decreases, larger GSC currents are required to achieve both FRT requirement and the elimination of second harmonic pulsations.

The negative and positive sequence fault currents (I_n and I_p) of the PV park in scenarios M1 and M2 are also quite different as illustrated in Figure 38. This difference strongly depends on the unbalanced fault type, its electrical distance to the PV park, GSC rating and the FRT requirement specified by the grid code. It becomes less noticeable especially for the electrical distant faults such as an unbalanced fault at BUS6 as presented in Section 5.1.2.

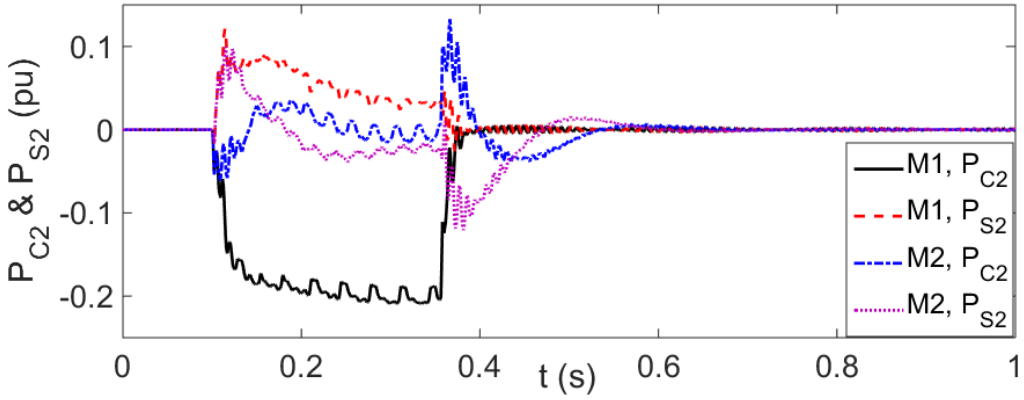

Figure 36 P_{C2} and P_{S2} of aggregated PV park in scenarios M1 and M2

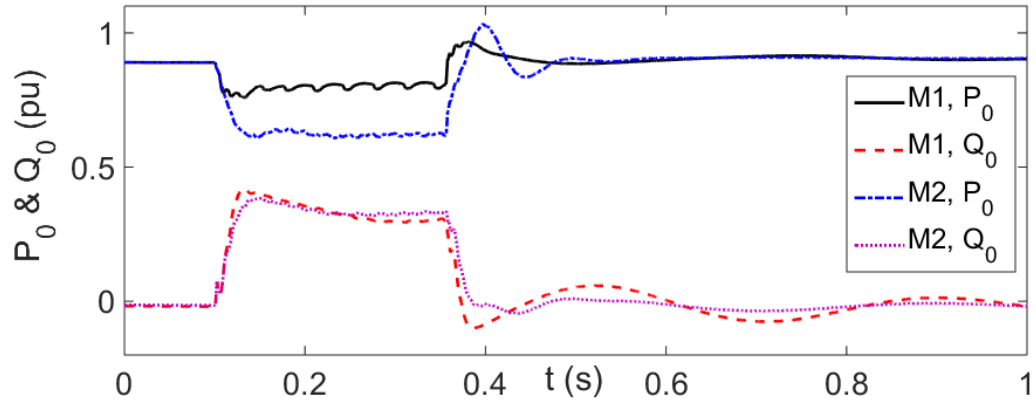

Figure 37 **P_0 and P_0 of aggregated PV park in scenarios M1 and M2**

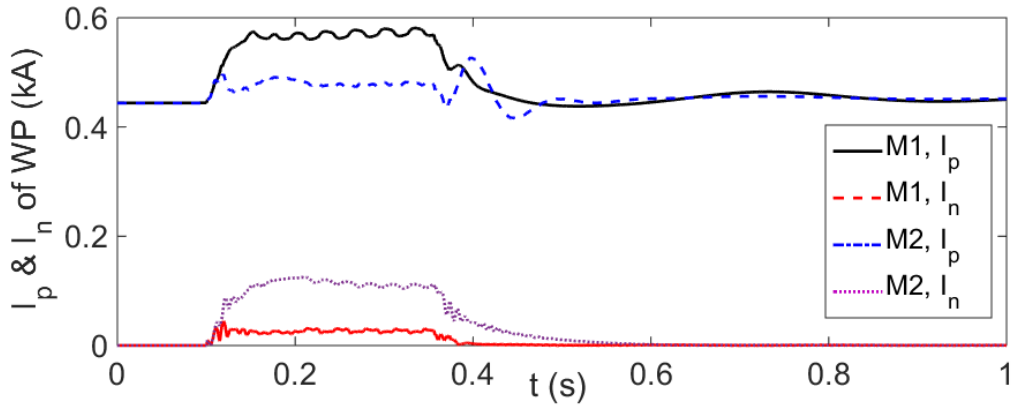

Figure 38 I_n and I_p of the PV park in scenarios M1 and M2

5.1.2 Simulation Scenarios N1 and N2 with the PV park

As the electrical distance between the PV park and the unbalanced fault is much larger in scenario N1 compared to scenario M1, both the voltage sag and the second harmonic pulsations in the active power output are much smaller in scenario N1 compared to the scenario M1 (see Figure 39 and Figure 36). As a result, the decupled sequence control of GSC achieves elimination of these pulsations in scenario N2 without any reduction in the active power output of the PV park (see Figure 40 and Figure **37**). As seen from Figure 41 and Figure 38, the PV park fault current contribution difference between the scenarios N1 and N2 also becomes less noticeable especially for positive sequence fault currents compared to the difference between scenarios M1 and M2.

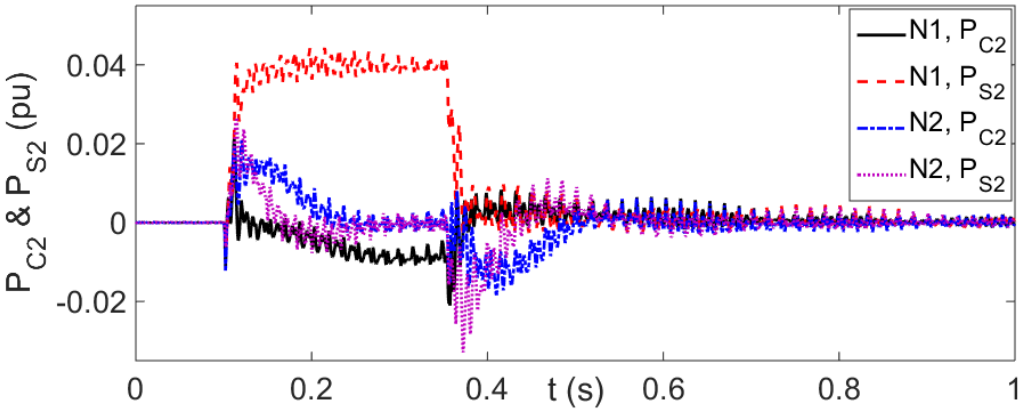

Figure 39 P_{C2} and P_{S2} of aggregated PV park in scenarios N1 and N2

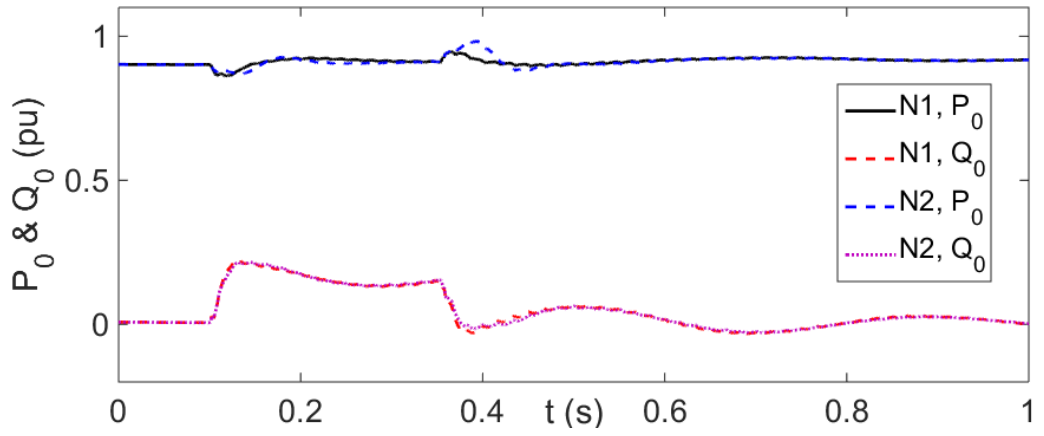

Figure 40 P_0 and Q_0 of aggregated PV park in scenarios N1 and N2

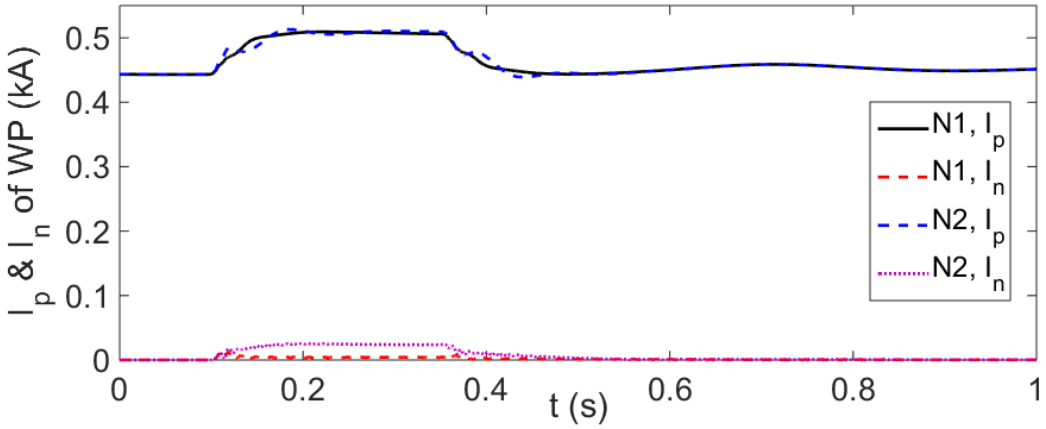

Figure 41 I_n and I_p of the PV park in scenarios N1 and N2

6 AVERAGE VALUE MODEL PRECISION AND EFFICIENY

6.1 120 kV Test System Simulations

This section provides a comparison between average value model (AVM) and detailed model (DM) of the presented PV park models. The simulation scenario M2 in Table I is repeated for 50 µs simulation time step (M3) and for DM with 10 µs simulation time step (M4).

6.1.1 Simulation Scenarios M2 - M4 with the PV park

As shown in Figure 42-Figure 44, AVM usage instead of DM provides very accurate results even for 50 µs time step usage.

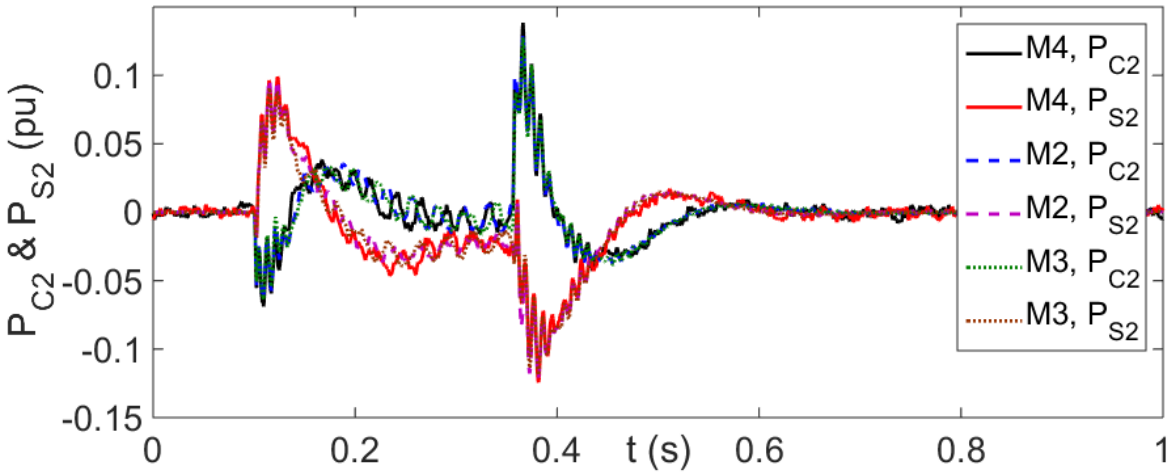

Figure 42 P_{C2} and P_{S2} of aggregated PV park in scenarios M2 - M4

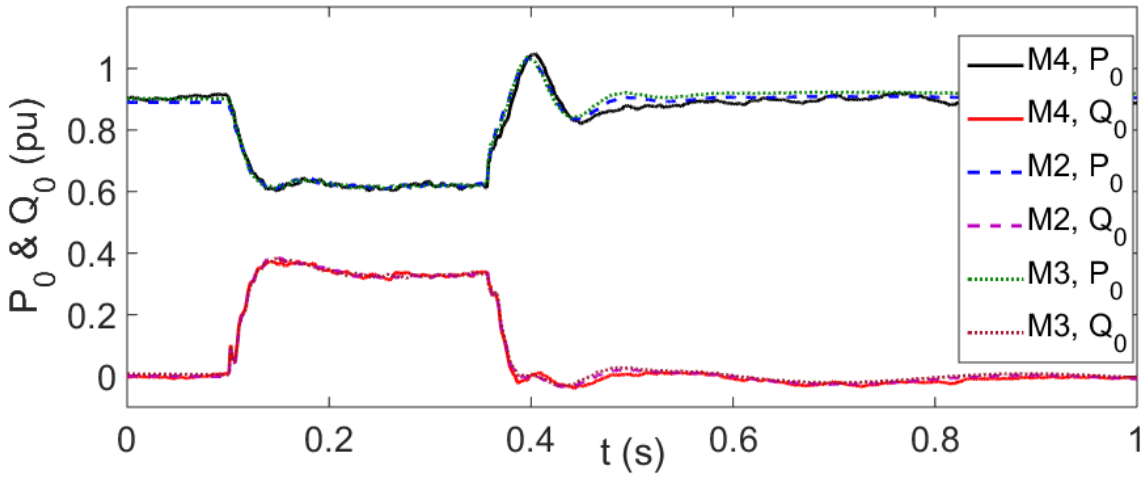

Figure 43 P_0 and Q_0 of aggregated PV park in scenarios M2 - M4

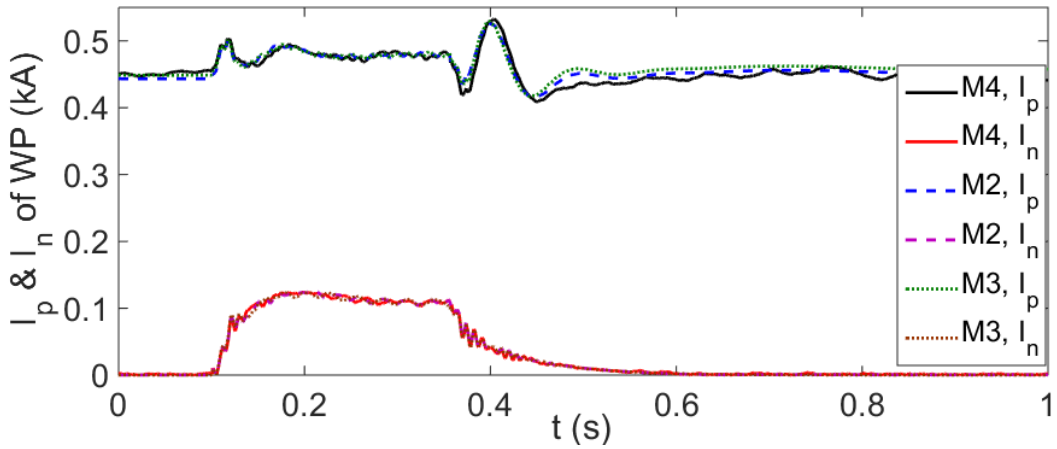

Figure 44 I_n and I_p of the PV park in scenarios M2 - M4

7 DETAILED PV PARK MODELS AND AGGREGATED MODEL PRECISION

The example is done with wind-turbines. The same conclusions can be drawn for PV park.

Certain grid integration studies, such as analysing collector grid faults and collector grid overcurrent protection system performance, LVRT and HVRT capability studies [4], ferroresonance study [32], require EMT type simulations with detailed Wind Park (WP) model. These studies do not only require detailed MW collector grid model, but also detailed model of HV/MV WP substation including overvoltage protection, overcurrent and differential current protections, measuring current and voltage transformers as shown in Figure 45 -Figure 47.

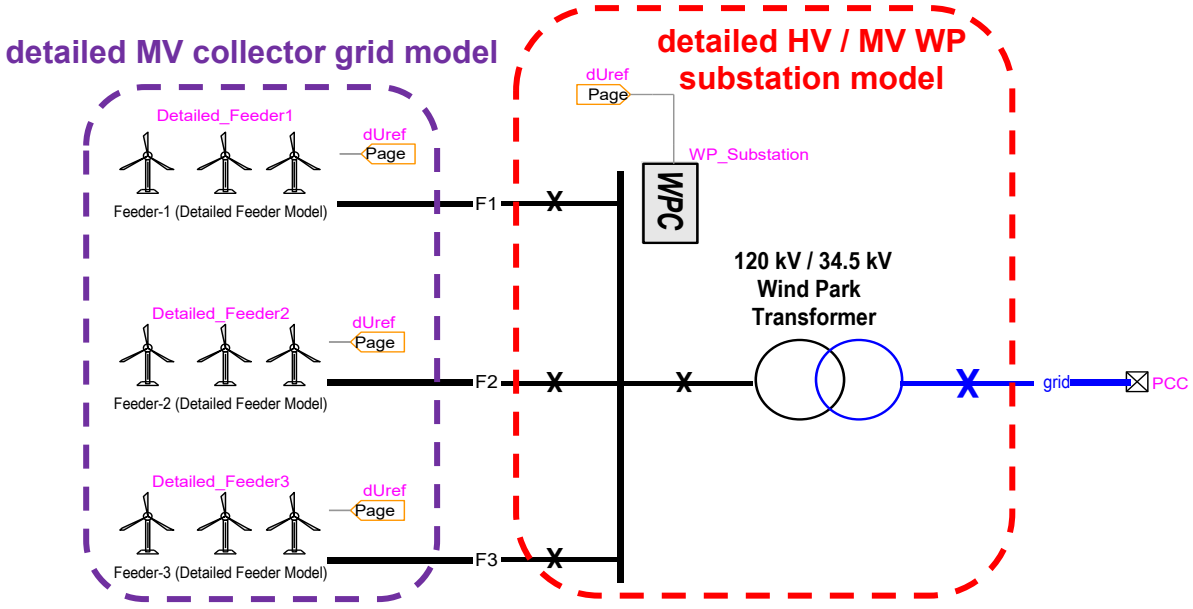

Figure 45 EMTP diagram of the 45 x 1.5 MW WP detailed model given in Figure 32.

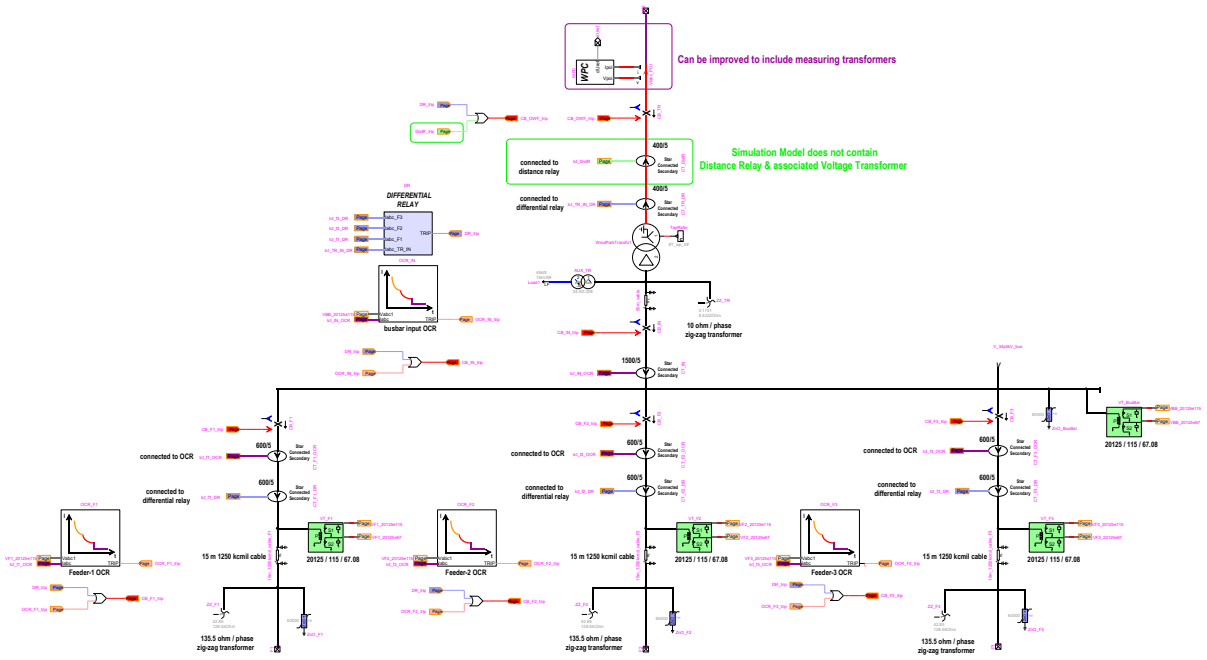

Figure 46 EMTP diagram of the HV/MV WP Substation

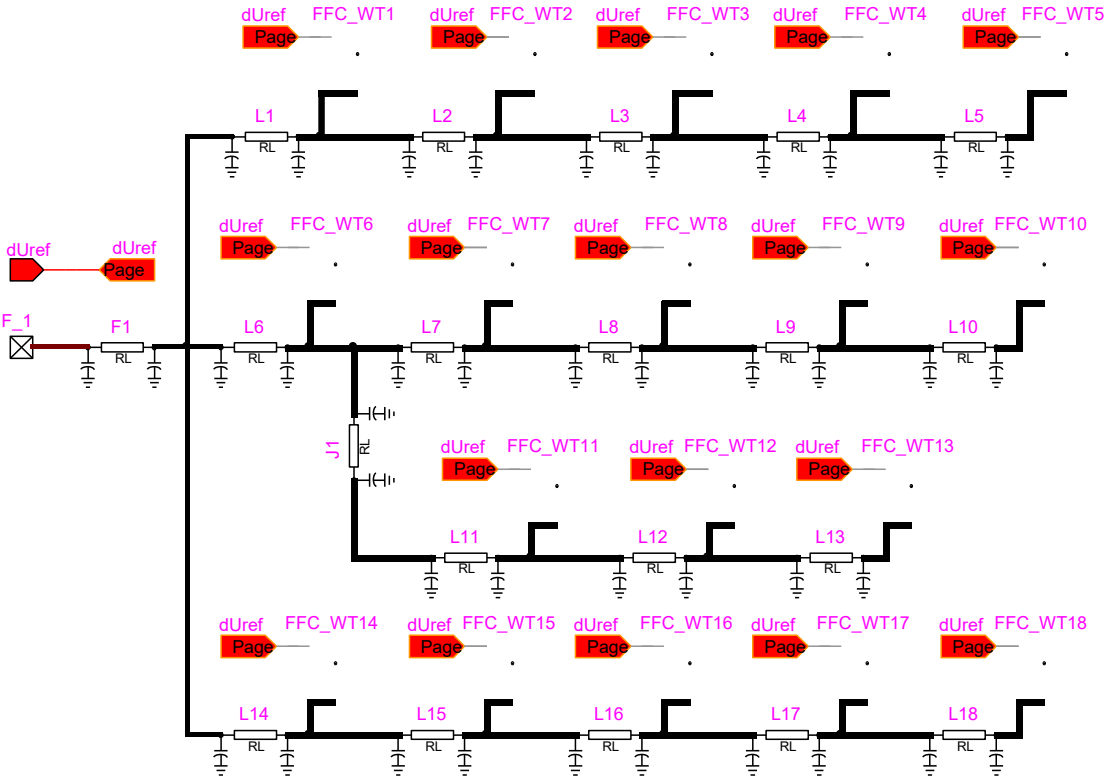

Figure 47 EMTP diagram of MV Feeder-1

The WT model in Figure 47 is obtained from the WP model presented in Chapter 4 by excluding the Wind Park Controller (WPC), WP transformer and collector grid equivalent. The associated device mask is shown in Figure 48. It does not include the tabs used for MV/HV WP transformer and WPC parameters. On the other hand, the first tab of the aggregated wind turbine mask includes certain WP parameters (total number of WTs in the WP, POI and collector grid voltage levels, collector grid equivalent and the MV/HV WP transformer impedances) in addition to the general wind turbine parameters (WT rated power, voltage and frequency) and wind speed. It should be noted that, the MV/HV WP transformer and the collector grid equivalent impedances are used GSC parameter calculation (see section 4.2.3.1).

Scenario M2 in Table I (DLG fault at BUS4 for GSC decoupled sequence control scheme) is simulated using the detailed WP model to conclude on accuracy of the aggregated model. As shown in Figure 49 - Figure 52, the aggregated models of WP provide accurate results.

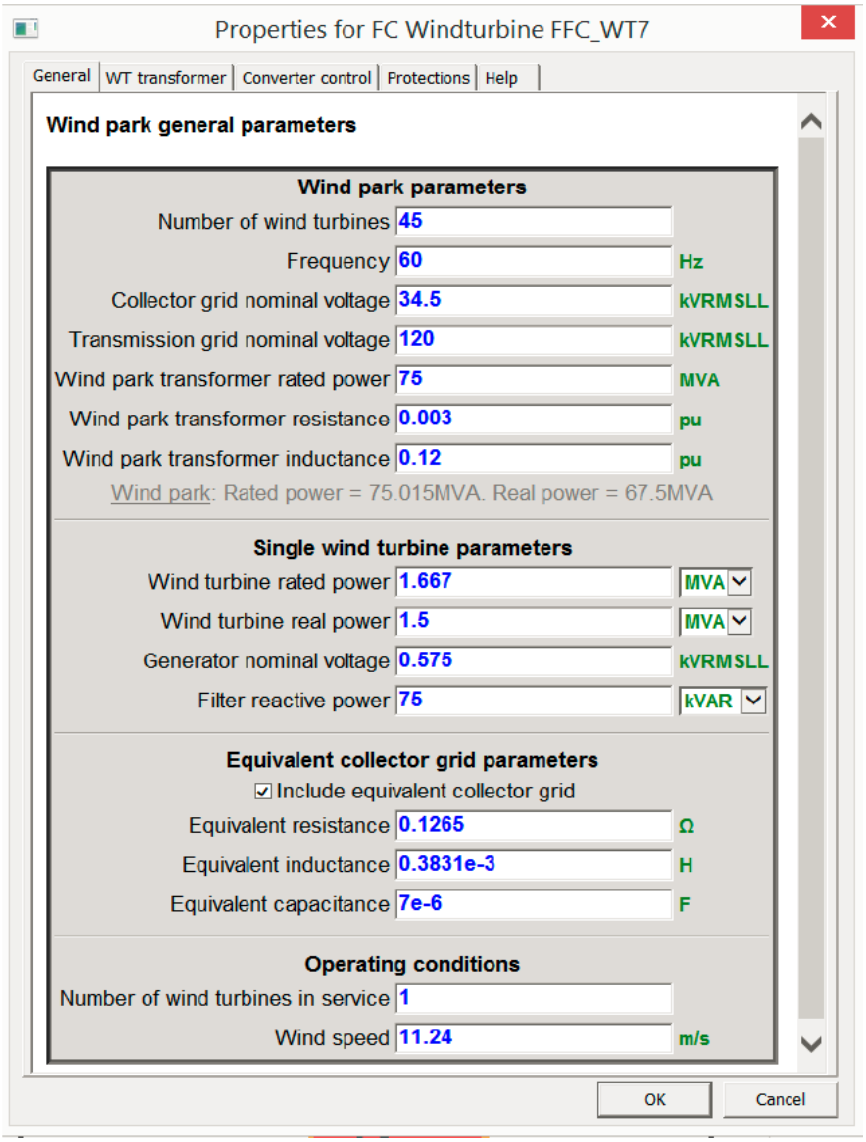

Figure 48 Aggregated FSC based wind turbine device mask

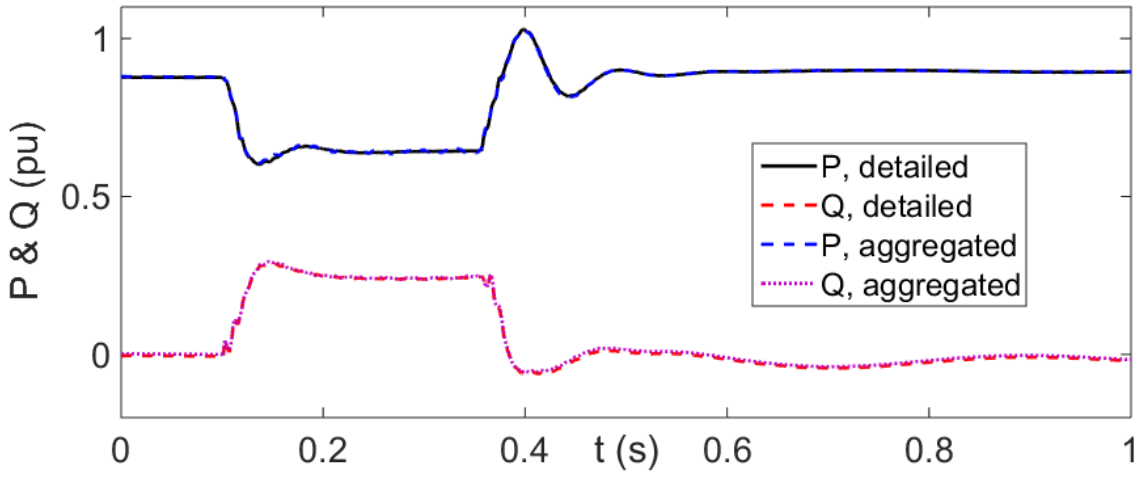

Figure 49 Active and reactive power at POI, PV park with FSC WTs

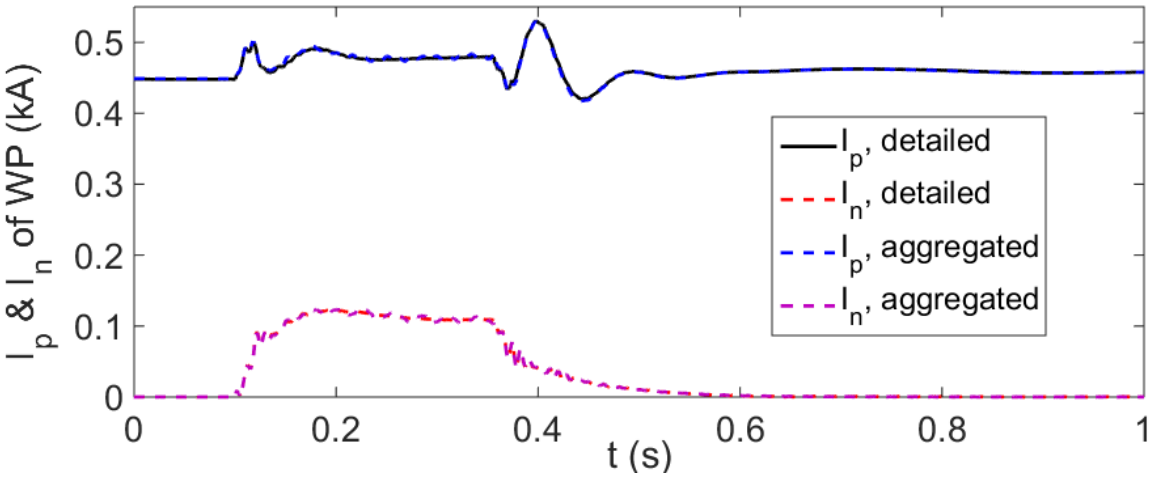

Figure 50 Positive and negative sequence currents at POI, PV park with FSC WTs

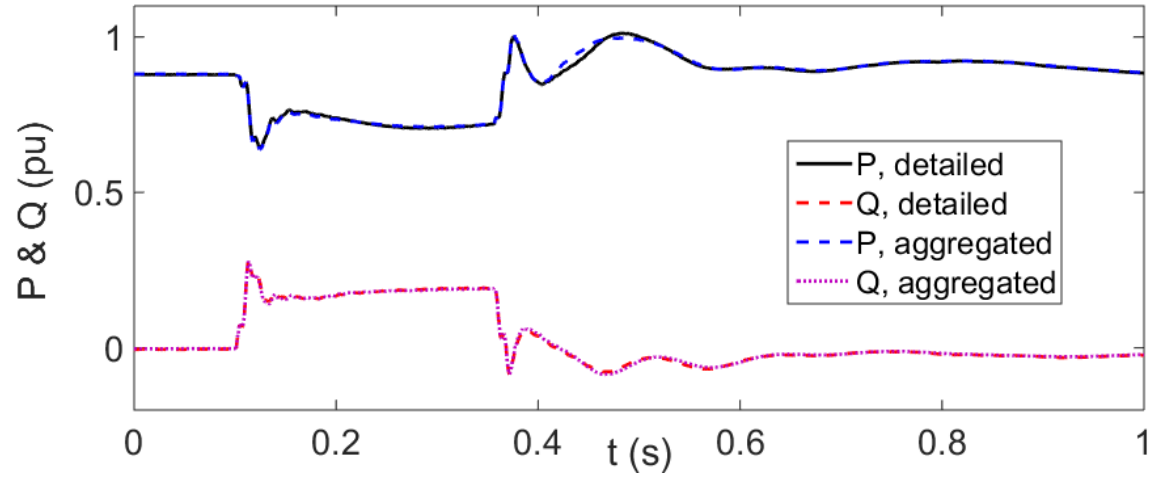

Figure 51 Active and reactive power at POI, PV park with DFIG WTs

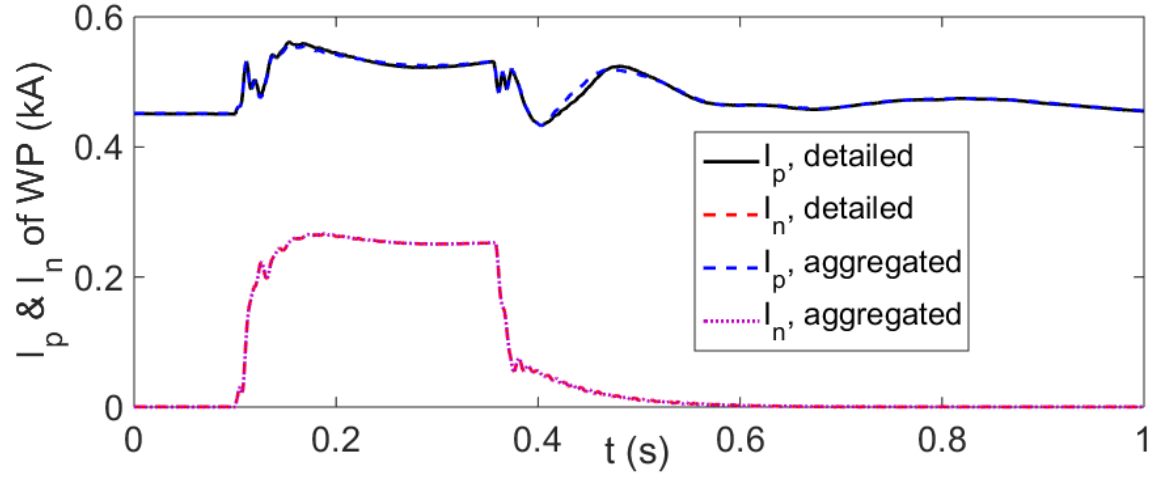

Figure 52 Positive and negative sequence currents at POI, WP with DFIG WTs

8 REFERENCES

[1] Chih Hao Chang, Jia-Jun Zhu and Huan-Liang Tsai. "Modelbased performance diagnosis for PV systems", SICE, 2010, pp. 2139-2145.

[2] G. H. Yordanov, O. M. Midtgård, T. O. Saetre, “PV Modules with Variable Ideality Factors”, in 38th IEEE Photovoltaic Specialists Conference, 2012, p. 002362.

[3] V. Sangsawang, S. Chaitusaney, “Modeling of Photovoltaic Module from Commercial Specification in Datasheet”, in 9th ECTI Conference, Phetchaburi, Thailand, May 16-18, 2012, pp. 1-4.

[4] U. Karaagac, J. Mahseredjian and L. Cai, “High Voltage Ride-Through Capability of DFIG-based PV parks with FACTS,” Proc. of 13th International Workshop on Large-Scale Integration of Wind Power into Power Systems, Berlin, Germany, Nov. 2014.

[5] O. Anaya-Lara, N. Jenkins, J. Ekanayake, P. Cartwright, and M. Hughes, Wind Energy Generation: Modelling and control, Wiley, 2009, John Wiley & Sons, Ltd.

[6] N. W. Miller, W. W. Price, and J. J. Sanchez-Gasca, “Dynamic modeling of GE 1.5 and 3.6 wind turbine-generators,” GE-Power System Energy Consulting, General Electric International, Inc., Schenectady, NY, USA, Oct. 2003.

[7] G. Abad, J. Lopez, M. A. Rodriguez, L. Marroyo, G. Iwanski, Doubly Fed Induction Machine: Modeling and Control for Wind Energy Generation, 2011, Wiley.

[8] M. Singh, S. Santoso, Dynamic Models for Wind Turbines and Wind Power Plants, 2011.

[9] J. M. Garcia, “Voltage control in wind power plants with doubly fed generators,” Ph.D. thesis, Alaborg Univ., Denmark, Sep. 2010.

[10] V. Akhmatov, A. H. Nielsen, J. K. Pedersen, O. Nymann, "Variable-speed wind turbines with multi-pole synchronous permanent magnet generators. Part I: Modelling in dynamic simualtion tools", Wind Eng., vol. 27, no. 6, pp. 531-548, Dec. 2003.

[11] S. R. Sanders, J. M. Noworolski, X. Z. Liu, and G. C. Verghese, “Generalized averaging method for power conversion circuits,” IEEE Trans. on Power Electron, vol. 6, no. 2, pp. 251–259, Apr. 1991.

[12] J. Morren, S. W. H. de Haan, P. Bauer, J. Pierik, and J. Bozelie, “Comparison of complete and reduced models of a wind turbine with Doubly-fed Induction Generator,” in Proc. 10th Eur. Conf. Power Electron. Appl., Toulouse, France, Sep. 2003.

[13] J. G. Slootweg, H. Polinder, and W. L. Kling, “Representing wind turbine electrical generating systems in fundamental frequency simulations,” IEEE Trans. on Energy Conv., vol. 18, no. 4, pp. 516-524, Dec. 2003.

[14] P. Rodriguez , J. Pou , J. Bergas , I. Candela , R. Burgos and D. Boroyevich, "Double synchronous reference frame PLL for power converters", Proc. IEEE PESC, pp. 1415-1421, 2005

[15] L. Harnefors and H. Nee, "Model-based current control of ac machines using the internal model control", IEEE Trans on Ind. Appl., pp. 133-141, Jan/Feb. 1998.

[16] “Grid code - high and extra high voltage,” E.ON Netz GmbH, Bayreuth, Germany, April 2006.

[17] R. Teodorescu, M. Liserre, P. Rodriguez, Grid Converters for Photovoltaic and Wind Power Systems, 2011, IEEE/Wiley.

[18] Rodriguez, P., Pou, J.,Bergas, J.,Candela, J. I.,Burgos,R.P. and Boroyevich, D., “Decoupled Double Synchronous Reference Frame PLL for Power Converters Control”, IEEE Transactions on Power Electronics, 22,March 2007, 584–592.

[19] Transmission Provider Technical Requirements for the Connection of Power Plants to the Hydro-Quebec Transmission System, Hydro Quebec Transenergie, 2009.

[20] G. R. Slemon, “Modelling of induction machines for electric drives,” IEEE Transactions on Industry Applications, 25(6):1126-31, 1989.

[21] R. Pena, J. C. Clare, G.M. Asher, “Doubly fed induction generator using back to back PWM converters and its application to variable-speed wind-energy generation”, IEE Proc. Electr. Power Appl., No.3. pp.231-240, 1996.

[22] Muljadi, T. Batan, D. Yildirim, C. Butterfield, “Understanding the unbalanced voltage problem in wind turbine generation Proc. Ind. Appl. Conf., pp. 1359–1365.

[23] T.K.A. Brekken, N. Mohan, “Control of a doubly fed induction wind generator under unbalanced grid voltage conditions,” IEEE Trans. Energy Convers., Vol: 22, No: 1, pp. 129-135, March 2007.

[24] L. Xu, Y. Wang, “Dynamic modeling and control of DFIG-based wind turbines under unbalanced network conditions,” IEEE Trans. Power Syst., Vol: 22, No: 1, pp. 314-323, Feb. 2007.

[25] R. Pena, R. Cardenas, E. Escobar, “Control system for unbalanced operation of stand-alone doubly fed induction generators,” IEEE Trans. Energy Convers., Vol: 22, No: 2, pp. 544–545, June 2007.

[26] H. Yin, L. Fan, R. Kavasseri, “Negative sequence compensation techniques of dfig-based wind energy systems under unbalanced grid conditions,” Proc. IEEE Power Electronics and Machines in Wind Applications (PEMWA), Lincoln, NE, 2009.

[27] L. Fan, H. Yin, Z. Miao, “A novel control scheme for DFIG-based wind energy systems under unbalanced grid conditions,” Electric Power Systems Research, Vol: 81, No:2, pp. 254–262, Feb. 2011.

[28] T. Kauffmann, U. Karaagac, I. Kocar, H. Gras, J. Mahseredjian, B. Cetindag and E. Farantatos, “Phasor Domain Modeling of Type III Wind Turbine Generator for Protection Studies,” Proc. of IEEE PES General Meeting, Denver, CO, USA, July 2015

[29] U. Karaagac, T. Kauffmann, I. Kocar, H. Gras, J. Mahseredjian, B. Cetindag and E. Farantatos, “Phasor Domain Modeling of Type-IV Wind Turbine Generator for Protection Studies,” Proc. of IEEE PES General Meeting, Denver, CO, USA, July 2015.

[30] T. Kauffmann; U. Karaagac; I. Kocar; S. Jensen; J. Mahseredjian; E. Farantatos, "An Accurate Type III Wind Turbine Generator Short Circuit Model for Protection Applications," in IEEE Trans. on Power Delivery, doi: 10.1109/TPWRD.2016.2614620.

[31] E. Muljadi, C.P. Butterfield, a Ellis, J. Mechenbier, J. Hochheimer, R. Young, N. Miller, R. Delmerico, R. Zavadil and J.C. Smith, "Equivalencing the collector system of a large wind power plant", 2006 IEEE PES General Meeting.

[32] U. Karaagac, J. Mahseredjian, L. Cai, “Ferroresonance conditions in PV parks”, Electric Power Systems Research, Vo: 138, pp 41-49, Sep. 2016.